IDŐJÁRÁS

QUARTERLY JOURNAL
OF THE HUNGARIAN METEOROLOGICAL SERVICE

CONTENTS

VOL. 120 * NO. 4 * OCTOBER – DECEMBER 2016

IDŐJÁRÁS

Quarterly Journal of the Hungarian Meteorological Service

Editor-in-Chief
LÁSZLÓ BOZÓ

Executive Editor
MÁRTA T. PUSKÁS

EDITORIAL BOARD

ANTAL, E. (Budapest, Hungary)
BARTHOLY, J. (Budapest, Hungary)
BATCHVAROVA, E. (Sofia, Bulgaria)
BRIMBLECOMBE, P. (Norwich, U.K.)
CZELNAI, R. (Dörgicse, Hungary)
DUNKEL, Z. (Budapest, Hungary)
FISHER, B. (Reading, U.K.)
GERESDI, I. (Pécs, Hungary)
HASZPRA, L. (Budapest, Hungary)
HORVÁTH, Á. (Siófok, Hungary)
HORVÁTH, L. (Budapest, Hungary)
HUNKÁR, M. (Keszthely, Hungary)
LASZLO, I. (Camp Springs, MD, U.S.A.)
MAJOR, G. (Budapest, Hungary)
MÉSZÁROS, E. (Veszprém, Hungary)
MÉSZÁROS, R. (Budapest, Hungary)
MIKA, J. (Budapest, Hungary)
MERSICH, I. (Budapest, Hungary)
MÖLLER, D. (Berlin, Germany)
PINTO, J. (Res. Triangle Park, NC, U.S.A.)
PRÁGER, T. (Budapest, Hungary)
PROBÁLD, F. (Budapest, Hungary)
RADNÓTI, G. (Reading, U.K.)
S. BURÁNSZKI, M. (Budapest, Hungary)
SZALAI, S. (Budapest, Hungary)
SZEIDL, L. (Budapest, Hungary)
SZUNYOGH, I. (College Station, TX, U.S.A.)
TAR, K. (Debrecen, Hungary)
TÄNCZER, T. (Budapest, Hungary)
TOTH, Z. (Camp Springs, MD, U.S.A.)
VALI, G. (Laramie, WY, U.S.A.)
WEIDINGER, T. (Budapest, Hungary)

Editorial Office: Kitaibel P.u. 1, H-1024 Budapest, Hungary
P.O. Box 38, H-1525 Budapest, Hungary
E-mail: journal.idojaras@met.hu
Fax: (36-1) 346-4669

Indexed and abstracted in Science Citation Index Expanded™ and Journal Citation Reports/Science Edition

Covered in the abstract and citation database SCOPUS®

Included in EBSCO's databases

Subscription by mail:
IDŐJÁRÁS, P.O. Box 38, H-1525 Budapest, Hungary
E-mail: journal.idojaras@met.hu

IDŐJÁRÁS

Quarterly Journal of the Hungarian Meteorological Service
Vol. 120, No. 4, October – December, 2016, pp. 353–364

An interpretation of the measured planetary radiation imbalance

György Major

Hungarian Meteorological Service
P.O.Box 38, H-1525 Budapest, Hungary
E-mail: major.gy@met.hu

(Manuscript received in final form May 31, 2016)

Abstract—Some time variation properties of the planetary imbalance are shown by using satellite measured radiation budget data. The covered period is 1962–2014. The data have been collected from publications and data bases. The solar incom part of the budget has been homogenized using new total solar irradiance (TSI) values. The positive imbalance increases as well as the time delay between the incoming and outgoing radiation.

Key-words: planetary imbalance, radiation budget, satellite measurements, TSI, response time

1. Introduction

The radiation budget of the planet Earth is

$$NET = TSI/4 - REF - OUT, \tag{1}$$

where:

- NET is the result of all radiation processes.
- TSI is the total solar irradiance, the number 4 is the ratio of the surface of the sphere to the cross section of the sphere perpendicular to the solar rays, this way TSI/4 is the planetary (global) average solar irradiation at the top of the atmosphere (incoming solar radiation: ICO). The shape of the Earth is not

exactly spherical, the rotational ellipsoid approximation gives 4.002 yearly ratio. *Loeb et al.* (2009) calculated 4.0034. In this work the spherical value is used. It is worth to mention that the few tenth of a percent correction is near to the uncertainity of recently measured TSI values.

- REF is the solar radiation reflected to the interplanetary space by the planet.
- OUT is the longwave radiation emitted to the interplanetary space by the planet. Its value is not a simple response to the incoming/absorbed one.

Eq. (1) does not contain the energy of cosmic rays and radio waves arriving to the Earth from the space, since their energy is negligible to the named ones.

If the climate of the planet is in equilibrium, the yearly average net radiation should be zero, that is the incoming and outgoing radiation is balanced, the possible imbalance should be short living small variations around zero.

To check the actual state of the radiation budget of the Earth, several experts have made serious efforts to construct instruments, develop data processing procedure, estimate the error of the received data, and analyze the received data provided by satellite-born instrumentation since the begining of the 1960's. Some early results directed to the global net radiation are the followings: *Ardanuy et al.* (1992), *Arking* and *Vemury* (1984), *Arking* (1996), *Ellis* and *VonderHaar* (1976), *Gruber* and *Winston* (1978), *Harrison et al.* (1993), *Jacobowitz et al.* (1984), *Kandel et al.* (1994), *Kyle et al.* (1985), *Kyle et al.* (1993), *Loeb et al.* (2009), *MacDonald* (1970), *Ohring* and *Gruber* (1983), *Randel* and *VonderHaar* (1990), *Raschke et al* (1973), *Raschke* (1968), *Spänkuch* (1995), *Stephens et al.* (1981), *VonderHaar* and *Raschke* (1972), *Winston* (1970). The latest global net radiation data are provided by the CERES (Cloud and the Earth's Radiatiant Energy System) project since March of 2000 (*Loeb,* 2015). This project uses all the previous experiences in instrument building, data processing, and personal knowledge, moreover, the data sampling is the best in the history of radiation budget measurements.

The values of yearly global net radiation provided by the above mentioned data sources are between +0.9 and + 5 W/m^2, that is during the past 5 decades, negative radiation imbalance did not exist according to the measured data series. The series were produced by several projects, and there were significant interruptions between the periods covered by different projects. Since the uncertainity of these net radiation data is equal or even larger than the values itself, climate scientists could not use these data series. According to the energy budget investigations of the full Earth system, these values do not fit the system, they are too high.

Using the GISS (Goddard Institut for Space Science) climate model *Hansen et al.* (2005) calculated the planetary radiative imbalance for the period of 1880–2005. From the begining the imbalance generally increases from zero to the order of 1 W/m^2, the increase interrupted by the volcanic eruption for 2–3 years, when the imbalance falls below even –2 W/m^2. The increase is slow

until 1960, afterward it is more significant. These results are in good agreement with the ocean heat content data. The heat capacity of oceans gives 93 percent of the planetary heat capacity, therefore, the planetary energy imbalance is almost equal to the change of the heat balance of the oceans.

Loeb et al. (2009) modified the original CERES data series creating the CERES EBAF (Energy Balanced And Filled) data series to eliminate the deviation between the satellite measured radiation imbalance and the ocean heat content data, moreover, they stated that the probable reason of the deviation is some kind of systematic calibration error of the satellite-born radiometers. This EBAF series has been constructed to serve the purposes of the climate system science.

In this work, the trends in both the EBAF and the previous satellite radiation budget data series are looked for.

2. Data

2.1. TSI

The TSI is not identical to the solar constant (the first solar constant measurement was made by Pouillet in 1838 from the surface), it contains the variations of incoming solar radiation that are due to variations in the solar activity. TSI measurements have been and are made separately from the measurement of other components of the radiation budget. Continuous satellite based TSI measurements are made from November 1978. The first group of modern (cavity) absolute pyrheliometers were constructed by the Eppley Laboratory (J. Hickey), the Jet Propulsion Laboratory (JPL, R. Willson), the Physical Meteorological Observatory Davos (PMOD, C. Fröhlich), and the Royal Meteorological Institut of Belgium (RMIB, D. Crommelynck). From these instruments a standard group is selected that defines the World Radiometric Reference (WRR), the recently official radiometric scale of the World Meteorological Organization (WMO). In 2003, the National Institut of Standards and Technology of USA (NIST) developed a corrected absolute pyrheliometer named Total Irradiance Monitor (TIM), that measures the TSI approximately by 6 W/m^2 lower than the previously mentioned first group. Recently, Finsterle (PMOD) and several collaborators develop the Cryogenic Solar Absolute Radiometer (CSAR) (*Finsterle,* 2015), that is an essentially different new absolute pyrheliometer in development phase. It seems that after 2018, the WMO shall have to decide amongst the above mentioned 3 pyrheliometric scales. Recently, most of TSI users accepts the NIST scale. In the time period of satellite-based planetary radiation budget measurements, only the development of the TSI measuring instrumentation is known precisely.

Some solar physicists groups connected the satellite-measured TSI data to solar models, and this way they constructed TSI data series backward to some

hundred years. For the period 1700–2000, *Dewitte* (2014) presented a TSI series. From this series we use the 1950–2000 section, but the values are decreased by 2.5 W/m^2 to transform them to the NIST scale. For the period 2000–2014 we accept the CERES Edition 4 TSI values (*Kratz et al.,* 2015), these are somewhat higher than the Edition 3A ones. In *Fig. 1,* the yearly mean TSI values are shown from 1950 to 2014.

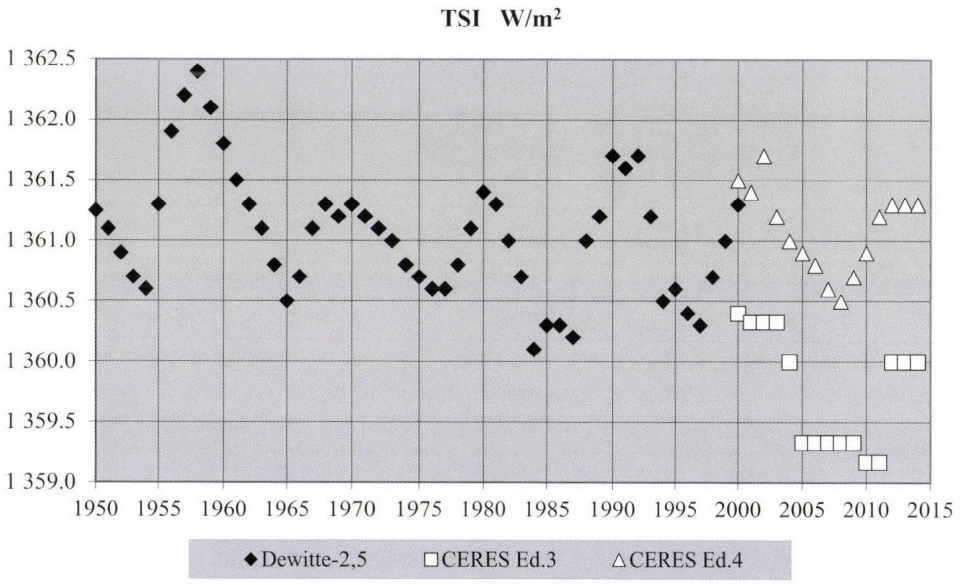

Fig. 1. The yearly TSI values used in this work. The 11 years sunspot cycle is seen clearly.

2.2. Radiation budget of 1962–1995

In *Table 1,* yearly or several yearly net radiation budget data are listed as they available from the named publications or data bases. This way, these data eliminate the variations arising from the yearly change of the Sun-Earth distance. Those published values that belong to period longer than 1 year has been composed from several monthly measured ones to represent the „mean" value of the period.

Table 1. Original data taken from publications and data bases. The numbers in parentheses are calculated from the original ones. Where not written, the unit is W/m^2. Earlier used unit: ly = langley = cal /cm^2.

Time period	Experiment	TSI	Reflected	Albedo	Absorbed	OUT	NET	ICO	Source
1962 – 1966 33 months	TIROS Nimbus-2 ESSA-7	1.95 ly/min		30.0%		0.34 ly/min	0.00 (0.9W/m^2)		*VonderHaar-Raeckhe*, 1972
1964 – 1971 29 months	TIROS Nimbus-2,3 ESSA-7 ITOS-1 NOAA-1	1360.0	103.3	32.4%	236.7	235.8	0.9	340.0	*Ellis-VonderHaar*, 1976
1964 – 1977 48 months	TIROS Nimbus-2,3,6 ESSA-3,7	1376.0		30.0%		232	9		*Stephens et al.*, 1981
1979	ERB	1372.7	(101.4)			235.8	6.0	(343.2)	*Ardanuy et al.*, 1992
1980	"	1373.3	(101.2)			236.3	5.8	(343.3)	"
1981	"	1372.0	(100.6)			236.4	6.0	(343.0)	"
1982	"	1371.7	(101.5)			235.4	6.0	(342.9)	"
1983	"	1371.7	(101.5)			235.9	5.5	(342.9)	"
1984	"	1371.3	(100.8)			235.4	6.6	(342.8)	"
1985	"	1371.5	(101.4)			234.9	6.6	(342.88)	"
1986	"	1371.4	(101.1)			235.2	6.6	(342.85)	"
1985	ERBE	(1362.4)		29.8%		234.0	5.1	(340.6)	Larc NASA S4G data
1986	"	(1362.8)		29.7%		234.0	5.5	(340.7)	"
1987	"	(1363.6)		29.5%		236.0	4.3	(340.9)	"
1988	"	(1368.4)		29.5%		237.0	4.2	(342.1)	"
1989	"	(1361.6)		29.7%		236.0	4.0	(340.4)	"
Mar-Sep, 1994 Nov-Dec, 1994 Jan-Feb,1995.	ScaRaB	(1366.0)		29.9%		237.0	2.4	(341.5)	ScaRaB CDs

In this work, the original radiation budget data have been corrected by substituting the original ICO or TSI data by using the TSI data shown in *Fig. 1*. The reflected solar radiation and the outgoing longwave radiation values are kept as in the original series. The corrected yearly imbalance data series is seen in *Fig. 2*. As a try of correcting the reflected and outgoing radiation data, *Shrestha et al* (2015) presented an improved ERBE series, but it is restricted to the 60N – 60S part of the globe.

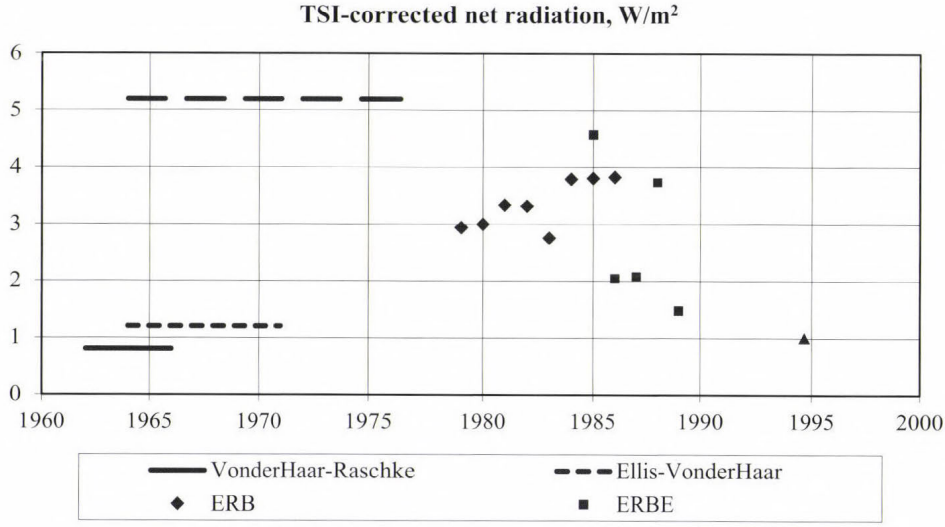

Fig. 2. The used imbalance data for 1964 – 1995. They are corrected to the TSI values seen in *Fig. 1*. The horizontal lines are characteristic to the covered period written in *Table 1*, the dots are calendar year means, except the ScaRaB point that is the mean of March 1994 –Febr 1995. The missing October is filled by interpolation.

2.3. Radiation budget of 2000–2014

Since the March of 2000, continuous high quality annual radiation budget data are available from the CERES Project (*https://ceres.larc.nasa.gov/products*). In this work, the CERES Ed.3A radiation data are used, except that the ICO of Ed.3A is changed to ICO of Ed.4 as mentioned in Section 2.1. The yearly (March-February) values are seen in *Fig. 3* altogether with the EBAF values. These Ed. 2.8 EBAF data are not corrected to the newer TSI (that is they contain the original Ed.3A ICO values), since the EBAF is fitted to the whole energy budget data of the climate system.

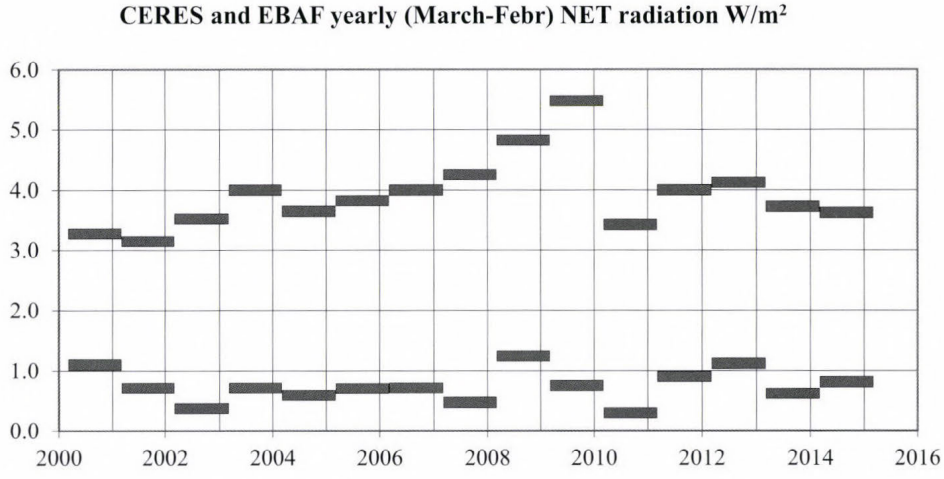

Fig. 3. The radiation balance data for the period of March 2000 – February 2015.

3. Time variations

3.1. The time period of March of 2000 – February 2014

This time period is covered the latest satellite-measured radiation budget data. Looking at *Fig. 3,* the most significant feature in the original CERES data series is the inreasing imbalance between 2000 and 2009, then a sudden decrease in 2010 and a weak increase afterward. The EBAF data do not show such strong variability, however, the year-to-year change is significant compared to the imbalance values itself. The basic statistics of the two series are printed in *Table 2.* Both linear trend coefficients show a slight (compared to the year-to-year variations) increase of the imbalance. In the increase of imbalance, the incoming solar radiation does not play important role, it is decreasing weakly, while the reflected and outgoing radiation are decreasing more significantly. Accordig to the standard deviations, the reflected solar and outgoing longwave radiation are not independent of each other.

Table 2. Basic characteristics of the March 2000 – February 2015 period according to the CERES and EBAF data series.

	EBAF			CERES		
	Mean W/m²	**Standard deviation W/m²**	**Trend $Wm^{-2}year^{-1}$**	**Mean W/m²**	**Standard deviation W/m²**	**Trend $Wm^{-2}year^{-1}$**
ICO	340.0	0.08	–0.0043	340.2	0.09	–0.0045
REF	99.7	0.20	–0.0083	97.9	0.51	–0.0486
OUT	239.6	0.24	–0.0019	238.8	0.24	0
NET	0.7	0.27	0.0059	3.5	0.60	0.0441

3.2. The time period of 1962 – 2014

The data seen in *Fig. 2* plus the original CERES data seen in *Fig. 3* are the satellite-measured yearly radiation imbalance of the last 5 decades. Taking them as one data series its basic statistical parameters are shown in *Table 3*. The trend parameters were calculated using the middle time point of the years or of the time periods the radiation values belong to. The planetary imbalance is increasing during this half century, while the year-to-year variation is much more significant similarly to the 2000 – 2014 period. If the idea of constant systematic calibration error of the satellite-born radiometers measuring the reflected solar and the outgoing longwave values is accepted for the whole period, then according to the high value of the regression coefficient of NET radiation, this error is not a simple additive one.

Table 3. Basic statistics for the period of 1962 – 2014

	Mean W/m²	**Standard deviation W/m²**	**Trend $Wm^{-2}year^{-1}$**
ICO	340.2	0.106	0.0017
REF	99.7	2.126	–0.1328
OUT	237.1	1.802	0.1006
NET	3.4	1.135	0.0339

4. Time delay between incoming and outgoing radiation

Fig. 4 shows the monthly CERES values of absorbed solar (short wave) and emitted longwave radiation. As it is expected, the yearly variations of the absorbed radiation (~ 15 W/m^2) exceed that of the emitted (long wave) ones (~ 8 W/m^2). The phase shift (response time) between the two waves is approximately a half year. The time delay between the absorbed and outgoing radiation depends not only on the thermal inertia of the planet but on the longwave transmissivity and emissivity properties of the atmosphere. The positive imbalance is seen clearly, the shortwave curve goes higher than the longwave one. Similar figure were prepaered by *Ardanuy et al.* (1992) for the period of 1979 – 1986.

The time delay (phase shift) between two waves could be measured by the time difference between the maxima and minima. Since the EBAF data fits better to the climate system than the original CERES ones, to quantify the response time between the planetary radiation income and outcome the differences of the dates of EBAF OUT yearly max and the yearly Perihelion, as well as that of EBAF OUT yearly min and the yearly Aphelion are taken. The astronomical dates have been obtained from http://aa.usno.navy.mil/data/EarthSeasons.php.

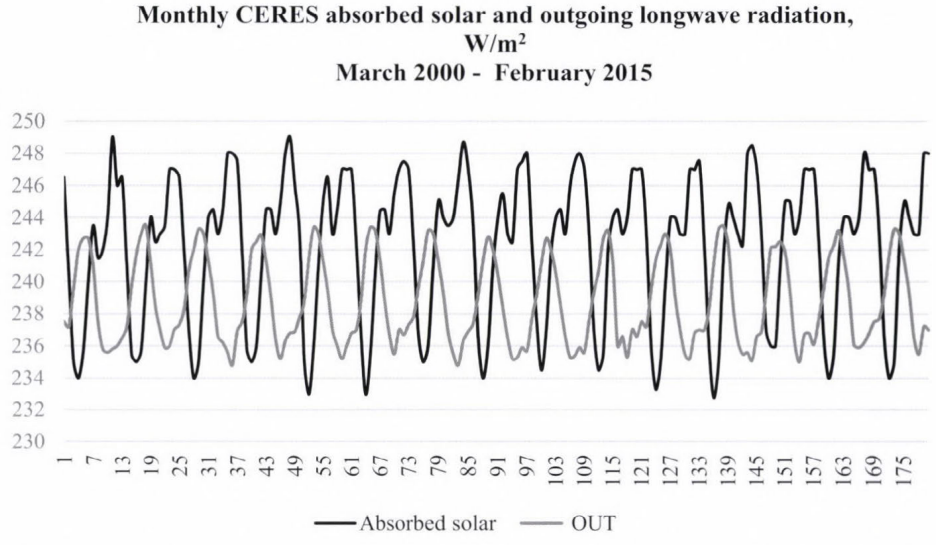

Fig. 4. Monthly global absorbed solar radiation and outgoing emitted radiation from the CERES data series.

Since the date of the peak values of OUT data are not well defined, two kinds of smoothing have been applied:

- the monthly values were taken into account instead of daily ones,
- a second order polinom were fitted to 5 monthly values around the expected dates, the dates of peak values of these polinoms were taken as peak dates of outgoing radiation.

In the outgoing radiation the dates of max peaks vary between July 23 and 31, while those of min peaks between December 29 and January 25. The first derived time difference between the max peaks has been established between the date of max OUT in July 2000 and the date of Perihelion in January 2000. The first one between min peaks has been derived from the date of min OUT in January 2001 and the date of Aphelion in July 2000. *Fig. 5* shows separately the 15 – 15 values between the maxima and minima. The linear trend gives a slight increase in both cases.

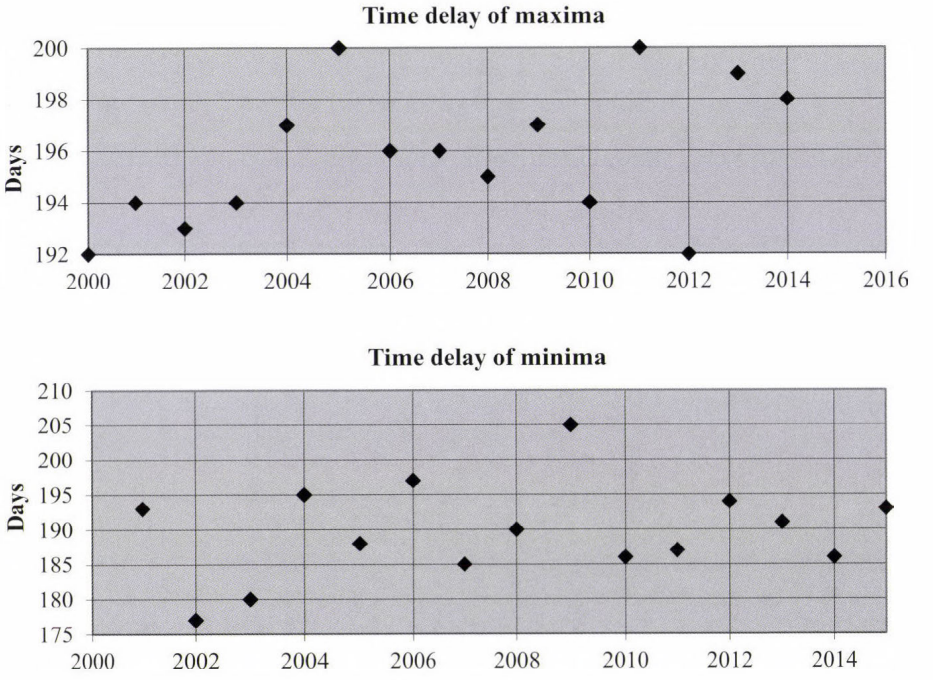

Fig. 5. Time difference (days) between the incoming solar radiation and the EBAF outgoing radiation. Upper panel: difference of max peaks, lower panel: that of min peaks.

5. Conclusion

More efforts would be necessary to correct the REF and OUT components of the radiation budget data measured by satellites before 2000 to better connect the planetary radiation imbalance to the global climate processes.

References

Ardanuy, P.E., Kyle, H.L. and *Hoyt, D.*, 1992: Global Relationship among the Eart's Radiation Budget, Cloudiness, Volvcanic Aerosols and Surface Temperature. *J. Climate 5*, 1120–1139.

Arking, A., 1996: Absorption of Solar Energy in the Atmosphere: Discrepancy Between Models and Observations. *Science 273*, 779–782.

Arking, A. and *Vemury, S.*, 1984: The Nimbus-7 ERB Data Set: A Critical Analysis. *J.Geophys Res. 89*, D4, 5089–5097.

Dewitte, S. 2014: The RMIB space odissey from Total Solar Irradiance to the Sun-earth IMBAlance (SIMBA). 23rd Science Team Meeting, October 6–10 2014, Toulouse ceres.larc.nasa.gov/science-team-meetings.

Ellis, J.S. and *VonderHaar, T.H.*, 1976: Zonal Average Earth Radiation Budget Measurements from Satellites for Climate Studies. Dept. Atm. Sci. CSU Paper No 240.

Finsterle, W. 2015: Status and future of the WRR in the SI. IPC-XII, 2015, PMOD/WRC Davos.

Gruber A. and *Winston J.S.* 1978: Earth-atmosphere radiative heating based on NOAA Scanning Radiometer measurements. *B. Am. Meteorol. Soc. 59*, 1570–1573.

Hansen, J., Nazarenko, L., Ruedy, R., Sato, M., Willis, J., Del Genio, A., Koch, D., Lacis, A., Lo, K., Menon, S., Novakov, T., Perlwitz, J., Russel, G., Schmidt, G.A., and *Tausnev, N.* 2005: Earth's energy imbalance: Confirmation and implications. *Science 308*, 1431–1435.

Harrison E.F., Minnis, P., Barkstrom B.R,. and *Gibson G.G.*, 1993: Radiation Budget at the Top of the Atmosphere. In: Atlas of Satellite Observations Related to Global Change. Cambridge University Press, London, 1993, CD Edition by NASA LARC. 19–38.

Jacobowitz H., Soule H.V., Kyle H.L., House F.B., and *the Nimbus-7 ERB Experiment Team*, 1984: The Earth Radiation Budget (ERB) Experiment: An Overview. *J.Geophys. Res. 89*, D4, 5021–5038.

Kandel R.S., Monge J.-L., Viollier M., Pakhomov L.A., Adasko V.I., Reitenbach R.G., Raschke E., and *Stuhlmann R.* 1994: The SCARAB Project: Earth Radiation Budget Observations from METEOR Satellites. *Adv. Space Res. 14*. 147–154.

Kratz, D.P., Gupta, S.K., Wilber, A.C., and *Sothcott, V.E.*, 2015: Status of the SOFA Validation and TSI Data. 24th Science Team Meeting, 4–9 May 2015, Hampton, Virginia, ceres.larc.nasa.gov/science-team-meetings.

Kyle, H.L, Ardanuy, P.E., and *Hurley, E.J.*, 1985: The Status of the Nimbus-7 Earth-Radiation-Budget Data Set. *B. Am. Meteorol. Soc. 66*, 1378–1387.

Kyle, H.L., Hickey, J.R., Ardanuy, P.E., Jacobowitz, H., Arking, A., Campbell, G.G., House, F.B., Maschhoff, R., Smith, G.L., Stowe, S.S., and *VonderHaar, T.H.*, 1993: The Nimbus Earth Radiation Budget (ERB) Experiment 1975 to 1992. *B. Am. Meteorol. Soc. 74*, 815–830.

Loeb, N.G., Wielicki, B.A., Doelling, D.R., Smith, G.L., Keyes, D.F., Kato, S., Manalo-Smith, N., and *Wong, T.*, 2009: Toward Optimal Closure of the Earth's. Top-of-Atmosphere Radiation Budget. *J. Climate 22*, 748–766.

Loeb, N.G., 2015: State of CERES. CERES Science Team Meeting, May 5–7, 2015, ceres.larc.nasa.gov/science-team-meetings2.php.

MacDonald, T.H., 1970: ESSA-7 Radiation Budget Data October 1968 – April 1969. Personal Communication.

Ohring, G. and *Gruber, A.*, 1983: Satellite radiation observations and climate theory. *Advan. Gerophys. 25*, 237–301.

Randel, D.L. and *VonderHaar, T.H.* 1990: On the Interannual Variation of the Earth Radiation Balance. *J. Climate 3*, 1168–1173.

Raschke E., 1968: The Radiation Balance of the Earth-Atmosphere System from Radiation Measurements of the Nimbus-2 Meteorological Satellite. NASA TN D-4589.

Raschke, E., VonderHaar T.H., Pasternak M., and *Bandeen, W.R.* 1973: The Radiation Balance of the Earth-Atmosphere System from Nimbus-3 Radiation Measurements. NASA TN D-7249.

Shrestha, A.K., Kato, S., Wong, T., Stackhouse, P.W., Rose, F., Miller, W.F., Bush, K., Rutan, D.A., Minnis, P. and *Doelling, D.*, 2015: Modeling ERBE WFOV Nonscanner dome degradation and reprocessing its radiation budget data from 1985 to 1998. CERES Science Team Meeting, September 1–3, 2015, ceres.larc.nasa.gov/science-team-meetings2.php.

Spänkuch, D., 1995: Die Strahlungseigenschaften der Erdamosphäre. *Sitzungberichte der Leibniz-Sozietät* 7(7). (In Deutsch)

Stephens, G.L., Campbell, G.G., and *VonderHaar, T.H.*, 1981: Earth Radiation Budgets. *J. Geoph. Res. 86*, 9739–9760.

VonderHaar, T.H. and Raschke, E. 1972: Measurements of the Energy Exchange Between Earth and Space from Satellites During the 1960's. Dept. Atm. Sci. CSU Paper No 184.

Winston, J.S. 1970: Radiation budget graphs March 1967 – February 1968. P*ersonal communication.*

IDŐJÁRÁS

Quarterly Journal of the Hungarian Meteorological Service
Vol. 120, No. 4, October – December, 2016, pp. 365–381

Changes in the structure of days with precipitation in Southern Poland in 1971-2010

Barbara Skowera[1]*, **Joanna Kopcińska J.**[2], and **Anita Bokwa**[3]

[1]*Department of Ecology, Climatology and Air Protection,*
Faculty of Environmental Engineering and Land Surveying,
University of Agriculture in Krakow,
24/28 Mickiewicza Av., 30-059 Krakow, Poland
E-mail: barbara196@interia.pl

[2] *Department of Applied Mathematics,*
Faculty of Environmental Engineering and Land Surveying,
University of Agriculture in Krakow,
253C Balicka St., 31-149 Krakow, Poland
E-mail:rmkopcin@cyf-kr.edu.pl

[3]*Institute of Geography and Spatial Management,*
Jagiellonian University,
7 Gronostajowa St., 30-387 Krakow, Poland
E-mail:anita.bokwa@uj.edu.pl

**Corresponding author*

(Manuscript received in final form January 13, 2016)

Abstract— In Poland, no clear tendencies have been detected in multi-year trends in precipitation sums. However, the number of days with precipitation has increased significantly. Therefore, we analyzed changes in the structure of days with precipitation, i.e., trends in the percentage of days with different ranges of daily precipitation sums. The precipitation data were from 1971–2010, from four stations in Southern Poland representing agricultural areas (Stare Olesno, Glubczyce, Lapanow, and Tuchow). Statistically significant upward trends (1–9 days per 10 years) and low variability were found for the number of days with daily precipitation sums up to 5 mm, mainly in the cold half of the year, and downward trends were found for days with 20–30 mm of precipitation (1 day per 10 years), with high variability. Comparison with the results of previous studies shows that the increase in the number of days with precipitation is not linked to a significant increase in precipitation sums.

Key-words: precipitation, Poland, trends, water resources, agriculture

1. Introduction

Changes in precipitation observed worldwide in recent decades are much more diversified regionally than changes in air temperature. The results presented in the Fifth Assessment Report of the IPCC *(Hartmann et al.,* 2013*)* show an overall increase in precipitation in the mid-latitudes of the Northern Hemisphere (30°N to 60°N) from 1901 to 2008, with statistically significant trends for each dataset used. For all other zones, due to data sparsity, poor data quality, and/or a lack of quantitative agreement among available estimates, characterization of such long-term trends in zonally averaged precipitation may be unreliable. Analyses of annual precipitation sums in Europe in the period 1960–2014, provided by the European Environmental Agency (*European Environmental Agency,* 2014*)*, show a decrease in Southern Europe (–37.07 mm per decade) and an increase in Northern Europe (20.64 mm per decade), both statistically significant. These tendencies were also found in earlier studies *(Schönwiese et al.,* 1997*; Brunetti et al.,* 2000*;, Førland* and *Hanssen-Bauer,* 1995*; Degirmendžić et al.,* 2004*; Klein Tank* and *Können,* 2003*; Bartholy et al.,* 2015*)*. Central Europe is located in a transitional zone. A study by *Niedźwiedź et al.* (2009) showed that precipitation in Central Europe fluctuates greatly in both time and space. No changing trend was found in any of the precipitation series studied, but a certain spatial regularity could be discerned. The test statistics change from a strongly negative value in Budapest to positive values that increase north-eastwards. These results are consistent with other studies covering smaller areas in Central Europe *(Domonkos* and *Tar,* 2003, *Kürbis et al,* 2009*; Tošić et al.,* 2016).

Previous studies of precipitation sums in Poland have not shown statistically significant changes *(Czarnecka and Nidzgorska-Lencewicz,* 2012*; Degirmendžić et al.,* 2004*)*. The authors of studies devoted to characteristics of the precipitation regime in Poland emphasize long-term fluctuations in the number of days with precipitation $\geq$0.1mm (*Degirmendžić et al.,* 2004*; Podstawczyńska,* 2007*; Wibig* and *Fortuniak,* 1998*; Bochenek,* 2012*; Skowera et al.,* 2014*)* and statistically significant upward trends in the number of days with precipitation *(Bochenek,* 2012*; Skowera et al.,* 2014*; Twardosz,* 2000). Therefore, the objective of this study was to analyze the multi-year variability in the structure of the number of days with precipitation, trends in the number of days with precipitation, and the role of days in particular classes of precipitation in determining the precipitation sum in the years 1971–2010, at stations representing agricultural areas in four regions of southern Poland. Regional aspects of both the structure of and trends in the number of days with precipitation are important in terms of formation of underground water resources and securing the precipitation needs of crop plants. Therefore, in this study we have considered all classes of precipitation sums. Agricultural regions of southern Poland, unlike in central and northern Poland, are located on diverse terrain, which in the case of atmospheric precipitation is an additional significant factor determining the spatial variability of this element.

Hence, in this study long-term changes in characteristics of the number of days with precipitation were considered with respect to the role of terrain relief.

2. Study areas

The data analyzed come from four meteorological stations, representing agricultural areas located in four mesoregions (following the division by *Kondracki* (2011)) belonging to two voivodeships (administrative regions) of southern Poland (*Fig. 1*). *Table 1* presents basic data on each station.

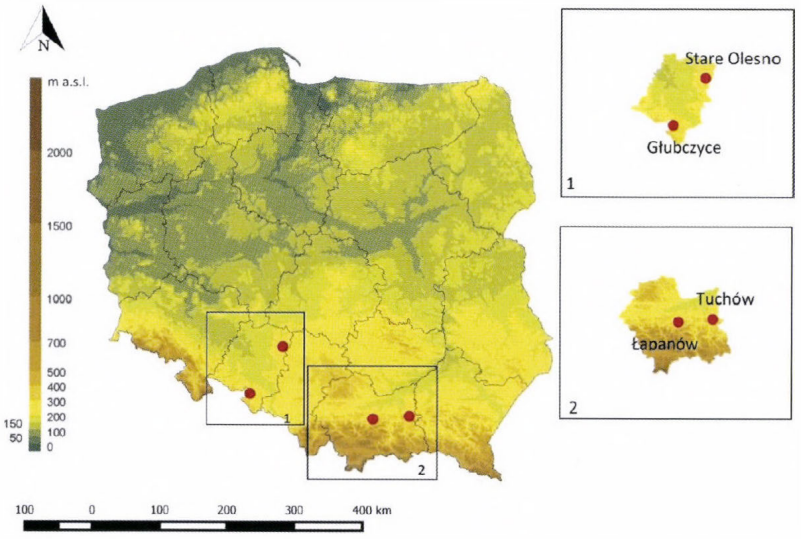

Fig. 1. Location of the Stare Olesno and Glubczyce in Opole Voivodeship (1) and Lapanow and Tuchow in Lesser Poland Voivodeship (1).

Table 1. Meteorological stations used in the study

Station	Voivodeship	Region	Coordinates	Altitude (m a.s.l.)
Stare Olesno	Opole	Woznicki cuesta	50°54′N 18°21E′	230
Glubczyce		Glubczyce Plateau	50°12′N 17°49′E	290
Lapanow	Lesser Poland	Wisnicz Foothills	49°52′N 20°19′E	236
Tuchow		Ciezkowice Foothills	49°54′N 21°03′E	235

As the spatial distribution of precipitation is highly dependent on the impact of land forms, both on a regional and a local scale, a short description of each mesoregion is provided. Woznicki cuesta, where the Stare Olesno station is located, is a low ridge running NW to SE. The mesoregion is located on the western border of the Woznicki-Wielun Upland. The neighboring region to the west and south is the Opole Lowland, and the difference in altitude between the regions is about 60 m. Glubczyce Plateau, where the Glubczyce station is located, is surrounded to the west by the Sudety Mountains. (altitude difference between the regions is about 1,000 m), and the neighboring region to the east is the Raciborz Basin (altitude difference is about 90 m). Lapanow and Tuchow are located in two foothill mesoregions belonging to the Carpathian Foothills, but Lapanow represents its western part and Tuchow its central part. Both stations are situated in river valleys (of the Stradomka River and the Biala River, respectively) which run south to north and are surrounded by hills (altitude about 400 m and 500 m a.s.l., respectively). Both mesoregions are surrounded by the Beskidy Mountains. to the south (altitude difference between the regions is about 1,000 m) and by the Sandomierz Basin to the north (altitude difference about 200 and 300 m, respectively). All four stations are located so as to represent the climatic conditions of the agricultural areas on a mesoregional scale. A factor contributing to the origin of precipitation in all study areas is the domination of western winds in Poland. As humid air masses bringing precipitation come from the west, the local land forms can enhance precipitation sums, acting as orographic barriers, or, conversely, can reduce precipitation sums in comparison to neighboring regions, i.e., create a rain shadow effect.

3. Materials and methods

In the study, we used the daily precipitation sums from 1971–2010 from the four meteorological stations described in Section 2. A day with precipitation was defined as a day with a daily precipitation sum ≥ 0.1 mm. The structure of days with precipitation was presented according to the criterion proposed by *Olechnowicz–Bobrowska* (1970). This method classifies days with precipitation according to daily precipitation sums in 6 classes:

0.1–1.0 mm: day with very light precipitation,

1.1–5.0 mm: day with light precipitation,

5.1–10.0 mm: day with moderate precipitation,

10.1–20.0 mm: day with moderately heavy precipitation,

20.1–30.0 mm: day with heavy precipitation,

> 30.0 mm: day with very heavy precipitation.

The number of days with precipitation was calculated in each class in successive months and half-years, i.e., the cold half of the year (October-March) and the warm half (April-September), and mean values were calculated for the period 1971–2010. The structure of days with precipitation was based on successive decades of the period 1971–2010 and presented as the percentage share of the number of days with precipitation of a given class during the year and for the warm and cold halves of the year. The warm half of the year is the growing season for plants and the time of work in the fields, and the cold half is the period of dormancy for crop plants. Coefficient of variation V (%) was calculated for days with a daily precipitation sum ≥ 0.1 mm and separately for each class of days with precipitation.

Trends in the number of days with precipitation were analyzed for each month and half-year. The Mann-Kendall test *(Kendall,* 1975*)* was used to verify whether we could reject the null hypothesis, that there is no trend in the sequence of data in favor of the alternative hypothesis of an upward or downward trend in the data y_i. The test determines whether the difference between a given element of the data sequence and a previous element is a positive or a negative value ($y_j - y_i$, where $j > i$) and assigns a value of 1 if the difference is positive, –1 if it is negative and 0 if it is 0. The statistic S was calculated as the sum of the integers according to the following formula:

$$S = \sum_{i=1}^{n-1} \sum_{j=i+1}^{n} \operatorname{sgn}(y_j - y_i), \tag{1}$$

where n is the total number of data.

The null hypothesis, that there is no trend in the data sequence, is rejected when the value of statistic S is significantly different from zero. We verify the null hypothesis on the basis of a normal Gaussian distribution, standardizing the statistic S according to the following formula:

$$Z = \begin{cases} \dfrac{S-1}{\sqrt{VAR(S)}} & S > 0 \\ 0 & S = 0, \\ \dfrac{S+1}{\sqrt{VAR(S)}} & S < 0 \end{cases} \qquad VAR(S) = \sqrt{\frac{n(n-1)(2n+5)}{18}}. \tag{2}$$

We reject the null hypothesis when the absolute value of statistic Z is greater than the theoretical value of the normal distribution $Z_{1-\frac{\alpha}{2}}$, where α is the level of significance. We adopted the values $\alpha = 0.05$ and $\alpha = 0.1$. The Z values are

$Z_{1-\frac{\alpha}{2}} = 1.95$ for $\alpha = 0.05$ and $Z_{1-\frac{\alpha}{2}} = 1.28$ for $\alpha = 0.1$. For data for which an upward or downward trend was found, the magnitude of the changes was estimated by calculating the Sen's slope estimator *(Hirsch et al.,* 1982) according to the following formula:

$$\beta = median\left(\frac{y_j - y_i}{j - i}\right), \quad \text{for } i < j\ ;\ i = 1, 2, \ldots, n\text{-}1, \quad j = 2, 3, \ldots, n. \tag{3}$$

Monthly, annual and semi-annual precipitation sums were also calculated, and then Spearman's rank coefficients were calculated between these sums and the number of days with precipitation in particular classes.

4. Results

Analysis of the structure of the number of days with precipitation in four regions of southern Poland in 1971–2010 revealed temporal and spatial variation in this characteristic of the precipitation regime. The highest mean annual number of days with precipitation was noted at the Stare Olesno station, with 171.3 days, and the lowest at the Glubczyce station, with 155.7 days (*Table 2*).

Table 2. Average number of days with precipitation per year and half-year in each precipitation class in 1971–2010.

Sum (mm)	Stare Olesno			Glubczyce			Lapanow			Tuchow		
	Year	Oct-Mar	Apr-Sep	Year	Oct-Mar	Apr-Sep	Year	Oct-Mar	Apr-Sep	Year	Oct-Mar	Apr-Sep
> 0.1	171.3	79.4	91.8	155.7	79.2	76.2	160.9	80.9	79.9	166.2	78.8	87.4
0.1 – 1.0	64.2	24.1	40.1	66.0	26.5	39.6	51.2	20.3	30.7	58.3	22.2	36.1
1.1 – 5.0	66.8	30.1	36.7	55.0	27.9	27.0	64.6	29.8	34.7	64.7	28.7	36.0
5.1 – 10.0	24.1	13.1	11.0	19.4	13.2	6.1	23.8	14.4	9.4	24.0	14.3	9.7
10.1 – 20.0	12.0	8.4	3.6	10.6	7.6	3.0	14.9	10.8	4.1	13.7	10.1	3.5
20.1 - 30.0	2.6	2.3	0.3	3.3	2.8	0.5	3.7	3.0	0.7	3.3	2.9	0.5
> 30.0	1.5	1.4	0.05	1.4	1.4	0.02	2.7	2.6	0.1	2.2	0.6	1.7

These differences can be attributed to the location of Glubczyce leeward of the Sudety Mountains., at their eastern foot. These mountains form an orographic barrier for moist polar air masses from the west. Precipitation is much lower to the east of the mountain range than to the west *(Kondracki,* 2011*)*. Stare Olesno is situated on a convex landform, where the precipitation is determined mainly by atmospheric circulation processes. The average annual number of days with precipitation at all stations during the study period was about 10-20 days higher than those reported by *Olechnowicz-Bobrowska* (1970) for the period 1951–1960. According to the *Atlas of the climate in Poland* (2005), in 1971–2000 the average annual number of days with precipitation >0.1 mm in the regions discussed was about 170, which was similar to the results obtained in our study. The number of days with precipitation >10 mm was also comparable. On an annual scale, light precipitation (class 1.1–5.0 mm) had the largest share in the structure of days with precipitation, with the exception of Glubczyce, where days with very light precipitation (0.1–1.0 mm) were dominant. In the warm half of the year, days with precipitation in the 0.1-1.0 mm class were dominant (except for Lapanow, with the greatest number of days in the 1.1–5.0 mm class), while in the colder half of the year, days with 1.1–5.0 mm dominated.

The structure of days with precipitation in successive decades of the study period is presented in *Figs. 2.1* and *2.2* for classes 0.1–1.0, 1.1–5.0, 5.1–10, and > 10.0 mm (the class of days with precipitation > 10.0 mm was introduced because the number of days in higher classes was small). Notable in this structure are the upward trends primarily in classes of days with very light and light precipitation in the cold half of the year and the variation in the number of days with precipitation between different meteorological stations in each decade.

The parametric Mann-Kendall test was used to verify whether the tendencies observed in changes in the structure of days with precipitation were statistically significant (significant trends $\alpha \leq 0.05$ and weak trends $0.05 < \alpha \leq 0.1$) (*Table 3.a*). Significant changes in very light precipitation (0.1–1.0 mm) were noted in Lapanow and Tuchow in both half-years and for the year, and in Glubczyce for the year and for the cold half of the year, while in Stare Olesno no trend coefficients were statistically insignificant. In Glubczyce, Lapanow, and Tuchow statistically significant trends were also noted in certain months, mainly in the cold half of the year. All statistically significant trends were upward; according to the Sen estimator, the number of days with precipitation in class 0.1–1.0 mm increased by about 1–9 per decade. In the case of higher classes, no significant trends were found in individual months and, therefore, for these classes the trends for the year and for each half-year are presented (*Table 3.b*). Statistically significant trends were noted only for classes 1.1–5.0 mm and 20.1–30 mm. In the case of class 1.1–5.0 mm these were upward trends, affecting only the number of days with such precipitation sums in Stare Olesno and Tuchow; for the year and the cold half-year they were about 2–3 days per decade. In the case of class 20.1–30.0 mm in Stare Olesno and Tuchow in the warm half of the year, a

decrease was noted of about 1 day per 10 years. In successive months of the warm half-year, no significant trends were found in the total number of days with precipitation (daily sum ≥0.1 mm) (*Table 4*).

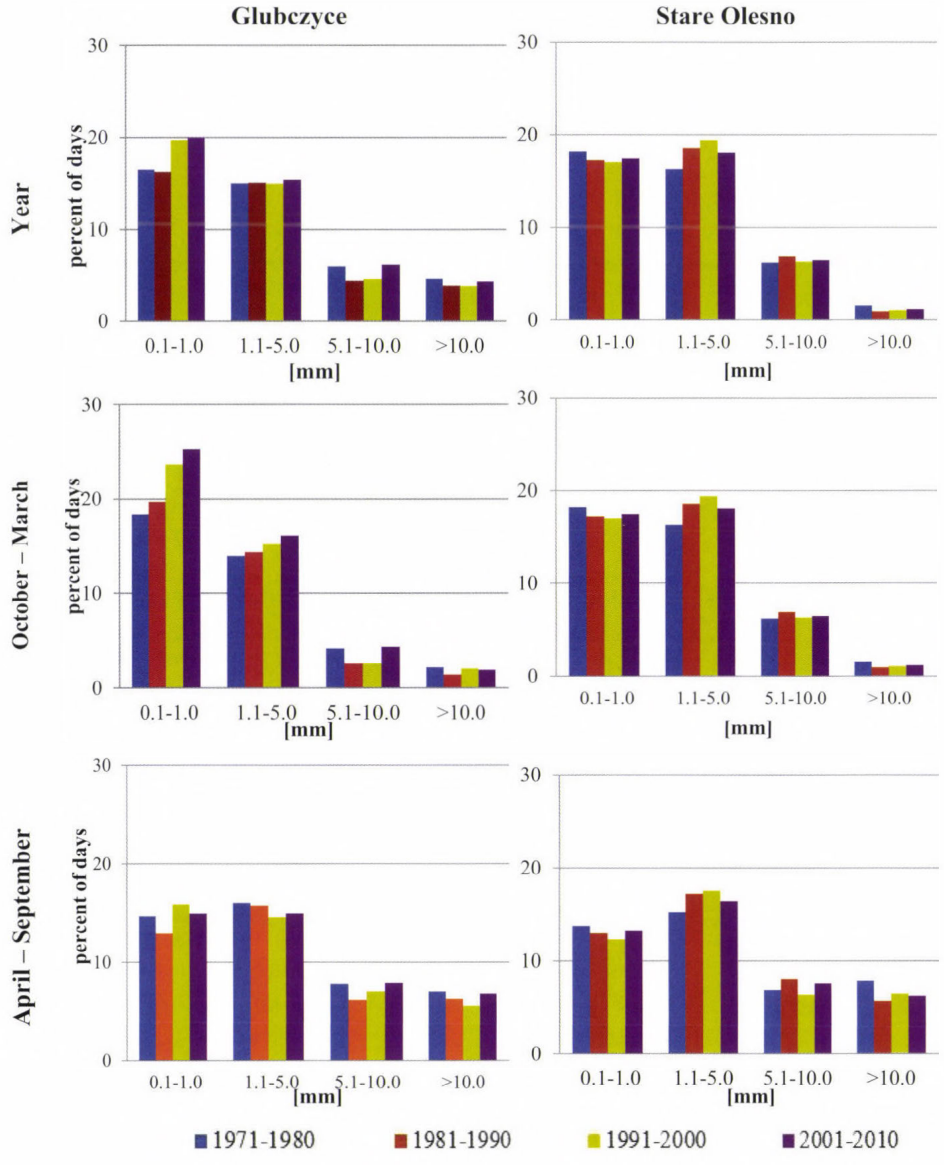

Fig. 2.1. Structure of days with precipitation (in successive decades) at selected stations in Opole Voivodeship in southern Poland (1971–2010).

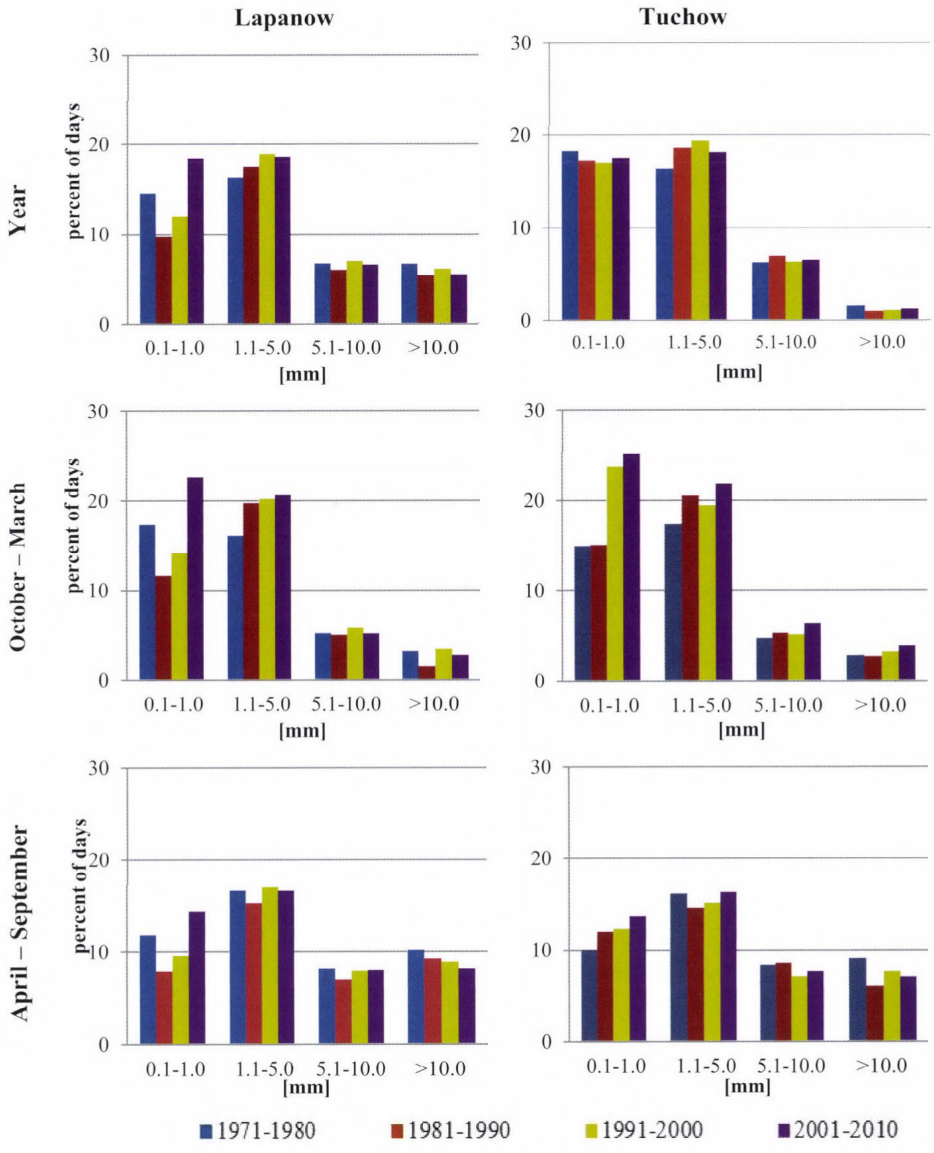

Fig. 2.b. Structure of days with precipitation (in successive decades) at selected stations in Lesser Poland Voivodeship in southern Poland (1971–2010).

Table 3.a. Trend coefficients for the number of days with precipitation |z| in 1971-2010: class 0.1–1.0 mm (individual months, half-years, and year)

Meteorological station	January	February	March	April	May	June	July	August	September	October	November	December	Year	Oct-Mar	Apr-Sep
Stare Olesno	0.53	0.20	-0.03	-1.47*	1.06	0.85	0.00	1.20	-1.05	0.47	-1.15	-0.24	0.52	-0.35	-0.05
Increase in days/10 years	-	-	-	-	-	-	-	-	-	-	-	-	-	-	-
Głubczyce	1.72*	3.40**	1.28	-0.30	-0.35	0.01	1.31*	0.34	-0.48	1.47*	2.88**	1.31*	2.81**	2.96**	1.41*
Increase in days/10 years	-	1.3	-	-	-	-	-	-	-	-	1.2	-	5.2	4.5	-
Lapanow	0.12	3.92**	0.66	2.07**	0.16	2.32**	0.79	1.02	0.76	0.76	2.11**	2.43**	2.74**	2.79**	2.16**
Increase in days/10 years	-	1.3	-	0.6	-	0.5	-	-	-	-	0.8	1.1	7.3	4.7	2.5
Tuchow	2.63**	2.92**	2.57**	0.17	1.59*	1.25	0.13	3.24**	1.28	3.01**	3.54**	2.63**	4.80**	4.57**	2.75**
Increase in days/10 years	2.69	1.0	0.8	-	-	-	-	1.4	-	1.4	1.3	0.8	8.2	6.3	2.0

Table 3.b. Trend coefficients for the number of days with precipitation |z| in 1971–2010: remaining classes of precipitation sums (half-years and year).

	1.1-5.0			5.1-10.0			10.1-20.0			20.1-30.0			>30.0		
Meteorological station	Year	Oct-Mar	Apr-Sep	Year	Oct-Mar	Apr-Sep	Year	Oct-Mar	Apr-Sep	Year	Oct-Mar	Apr-Sep	Year	Oct-Mar	Apr-Sep
Stare Olesno	2.54**	2.38**	0.42	0.23	0.54	-0.70	0.34	0.26	-0.13	-2.82**	0.08	-3.48**	1.09	0.00	0.00
Increase in days/10 years	3.3	2.5	-	-	-	-	-	-	-	-0.6	-	-0.6	-	-	-
Głubczyce	0.36	1.05	-0.60	0.04	-0.44	0.15	0.31	-0.21	0.49	-0.77	-0.27	-0.63	0.54	0.00	0.00
Increase in days/10 years	-	-	-	-	-	-	-	-	-	-	-	-	-	-	-
Lapanow	1.60*	1.66*	0.18	-0.38	-1.12	0.35	-0.61	0.17	-1.29*	-1.65*	-0.02	-2.30**	-0.05	0.00	0.00
Increase in days/10 years	-	-	-	-	-	-	-	-	-	-	-	-0.7	-	-	-
Tuchow	2.61**	2.30**	0.43	-0.36	1.28	-1.44*	-0.68	0.48	-0.67	-0.76	0.31	-0.48	*1.80**	*3.70***	*-2.27***
Increase in days/10 years	2.9	2.3	-	-	-	-	-	-	-	-	-	-	-	*0.5*	*0*

Statistical significance: ** - for $\alpha = 0.05$ with $|z| > 1.95$; * - for $\alpha = 0.1$ with $|z| > 1.28$

Italics indicate values, which due to the small number of cases of days with precipitation >30mm (despite significant values for statistic |z|) can not be treated as reliable

Table 4. Trend coefficients for the number of days with precipitation > 0.1mm in 1971–2010

Meteorological station	January	February	March	April	May	June	July	August	September	October	November	December	Year	Oct-Mar	Apr-Sep
Stare Olesno	1.38*	1.61*	1.29*	–1.61*	0.98	-0.21	0.13	1.72*	–1.37*	0.29	–0.16	–0.39	1.06	1.14	–0.31
Glubczyce	0.81	2.93**	1.53*	–0.64	0.75	–0.50	0.96	–0.16	–0.62	1.24	2.32**	0.23	2.68**	2.67**	–0.07
Lapanow	1.34*	2.58**	2.53**	0.52	0.88	0.70	0.63	–0.47	0.16	0.79	0.76	0.85	2.58**	2.62**	0.81
Tuchow	2.71**	2.86**	2.47**	1.01	1.04	0.09	0.08	1.71*	–0.01	1.74*	2.34**	1.08	4.80**	4.83**	1.04

Statistical significance: ** for $\alpha = 0.05$ for $|z| > 1.95$; * for $\alpha = 0.1$ for $|z| > 1.28$

A characteristic feature of the precipitation sums and the number of days with precipitation in the regions studied is the considerable variability from year to year. As in the case of the trends, the coefficient of variation in each precipitation class was calculated for the year and for both half-years-warm and cold. Following *Sobczyk* (2009): a value >20% was taken to mean that a given population is significantly varied in terms of the trait analyzed. The coefficient of variation of the annual number of days with precipitation (daily sum ≥0.1 mm) ranged from 10% at the stations located in the Opole Voivodeship to 11–12% in the Lesser Poland Voivodeship. In the warm half-year at all stations, the variability of this characteristics ranged from 13% to 15% and was somewhat lower than in the colder half of the year, i.e., from 15% to 19%, which means small variation in annual and semi-annual numbers of days with precipitation. However, the variability in monthly numbers of days with precipitation was much greater. The highest variation in the number of days with precipitation at all stations was noted for October (38–44%), while the lowest variation for this trait (about 26–27%) occurred in different months at different stations. The lowest variation was found for the number of days with light precipitation (1.1–5.0 mm: 11–25%), followed by very light (0.1–1.0 mm: 16–31%) and moderate (5.1–10.0 mm: 21–42%) precipitation. In the higher classes (>10 mm), the variation in the number of days was much greater, at 25–67%, and in the case of these classes, greater variation between seasons can be seen. In the cold half of the year, the coefficient of variation reached a value of 45–67%, and in the warm half, 29–33% (*Table 5*).

Table 5. Coefficient of variation for mean annual and seasonal numbers of days with precipitation (%) in the classes distinguished, in the period 1971-2010 at the stations studied

Sum (mm)	Stare Olesno			Glubczyce			Lapanow			Tuchow		
	Year	Apr-Sep	Oct-Mar	Year	Apr-Sep	Oct-Mar	Year	Apr-Sep	Oct-Mar	Year	Apr-Sep	Oct-Mar
>0.1	10	13	15	10	14	18	12	15	17	11	13	19
1.1–1.0	16	20	20	17	20	25	27	31	31	24	23	30
1.1–5.0	14	20	22	13	20	22	14	25	22	11	17	21
5.1–10.0	21	33	29	29	34	38	27	28	42	22	28	36
>10.0	58	31	66	28	33	62	25	29	67	28	32	45

Table 6 presents correlations between the number of days with precipitation in individual classes and annual and semi-annual precipitation sums. At all stations, the precipitation sum in both seasons was significantly influenced by the number of days with precipitation in classes > 10 mm, and in the cold half of the year, the precipitation sum was also significantly influenced by the number of days with precipitation in lower classes.

Table 6. Correlations between the number of days with precipitation in a given class (mm) and the precipitation sum in the year and half-years in 1971-2010

Meteorological station	Period	>0.1	0.1-1.0	1.1-5.0	5.1-10.0	10.0-20.0	20.1-30.0	>30.0
Stare Olesno	Year	0.47*	0.02	0.12	0.11	0.62*	0.39*	0.61*
	Apr-Sep	0.57*	0.28	0.01	0.30	0.56*	0.51*	0.56*
	Oct-Mar	0.56*	-0.04	0.58*	0.61*	0.72*	0.34*	0.34*
Glubczyce	Year	0.46*	0.09	0.22	0.47*	0.22	0.63*	0.59*
	Apr-Sep	0.46*	0.01	0.32*	0.29	0.34*	0.55*	0.60*
	Oct-Mar	0.32*	0.04	0.43*	0.23	0.35*	0.48*	-0.05
Lapanow	Year	0.51*	0.25	0.20	0.48*	0.34*	0.40*	0.74*
	Apr-Sep	0.53*	0.11	0.15	0.28	0.54*	0.47*	0.72*
	Oct-Mar	0.72*	0.36*	0.38*	0.49*	0.64*	0.46*	0.22
Tuchow	Year	0.51*	0.09	0.26	0.59*	0.50*	0.63*	0.63*
	Apr-Sep	0.63*	0.07	0.34*	0.32*	0.57*	0.56*	0.31*
	Oct-Mar	0.51*	0.15	0.46*	0.63*	0.72*	0.33*	0.17

* significant correlation coefficient ($\alpha = 0.05$)

5. 5. Discussion

The results presented show that in all the regions similar tendencies were observed in changes in the structure of the number of days with precipitation, with certain aspects of these tendencies modified by local environmental conditions. In the structure of the number of days with precipitation, days with precipitation sums < 5 mm, i.e., very light and light, are dominant. They show a statistically significant upward trend and, at the same time, little variation over the long term. This increase is observed mainly in the cold half of the year, both in the entire half-year and in some of its months. Moreover, the number of days with daily

precipitation sums < 5 mm has a significant role in determining the precipitation sum, mainly in the cold half of the year. For days with higher daily precipitation sums, including for extreme precipitation, either no statistically significant trends in changes are observed or the trends are downward. *Lupikasza* (2010) summed up studies of changes in extreme precipitation in Europe and in Poland and found that 'during summer time, any positive trends in extreme precipitation observed in Europe are much weaker than those found in winter time and are mostly statistically insignificant. Indeed, significant negative trends have been identified in many areas of Europe in summer time' and 'during 1951–2006, decreasing trends in extreme precipitation indices dominated in both the warm and cool halves of the year and in the seasons in Poland.' The results of our study in southern Poland are thus consistent with the tendencies observed in *Lupikasza's* study (2010), as well as with results obtained by *Bartholy et al.* (2015) for Hungary, *Moberg et al.* (2006) and *Rodrigo* (2010) for Europe. At all stations, the number of days with precipitation > 10 mm showed either no statistically significant trends in changes or downward trends, and at the same time, the highest long-term variation. Moreover, days with precipitation > 10 mm have a significant role in determining the precipitation sums in the year and in half-years. In terms of water resources for agriculture, the tendencies presented indicate a direction of changes in the precipitation regime that can be considered unfavorable. The climate scenarios presented in the IPCC report *(Kirtman et al.,* 2013*)* suggest that in 2016–2035, in comparison with 1986–2005, seasonal precipitation sums in the regions studied in Poland will be about 5% lower in the summer and 5% higher in the winter. A significant factor is the considerably greater long-term variability in the number of days with precipitation > 10 mm than in the number of days with precipitation < 5 mm. In the cold half of the year, which covers the beginning and end of the growing season, we can expect the precipitation demands of crop plants to be met, while during most of the growing season we can expect a shortage, due to the lower number of days with precipitation, high variability in the frequency of days with high and extreme precipitation, and lower precipitation sums. Previous studies have shown that due to increased air temperature, in some mesoregions of Poland, rainfall deficits in the spring have been more frequent than the excessive rainfall for crops (*Skowera et al.,* 2014). The number of days with precipitation determines the distribution of precipitation supply over time. In the years 1971–2010, a downward tendency was observed in the number of precipitation spells in the warm half of the year (Glubczyce) and an increase in the cold half of the year (Lapanow and Tuchow) (*Skowera* and *Wojkowski,* 2015). Given that in the cold half of the year the number of days with very light precipitation increased while no increase was observed in the precipitation sum, we can conclude that the observed change in the structure of the number of days with precipitation did not translate to an increase in post-winter water resources for crop plants.

6. Conclusion

Most studies of the number of days with precipitation focus on extreme precipitation, while precipitation with lower daily sums is overlooked.

The results presented regarding the structure of the number of days with precipitation in southern Poland demonstrate the significant role of the number of days with very light (0.1–1.0 mm) and light precipitation (1.1–5.0 mm) in determining precipitation sums (particularly in the cold half of the year) and water resources for agriculture. In the period 1971–2010, changes in precipitation sums showed no significant tendencies, but an increase was observed in the number of days with very light and light precipitation and a decrease in the number of days with 20.1–30.0 mm of precipitation. The magnitude of these changes varied between stations. In light of the anticipated climate changes in Europe, precipitation in southern Poland will undergo slight changes in the next few decades, similar to those observed until now, but with a tendency towards a decrease in precipitation in the summer and an increase in the winter. If the tendency in the change in the number of days with precipitation does not change, we can expect a further increase in the number of days with very light and light precipitation, particularly in the cold half of the year, and a decrease in the number of days with 20–30 mm of precipitation in the summer period.

Acknowledgements–Research was supported by the Ministry of Science and Higher Education of Republic of Poland through the core funding for statutory R&D activities

References

Bartholy, J., Pongrácz, R., and *Kis, A.,* 2015: Projected changes of extreme precipitation using multi-model approach. *Időjárás 119*, 129–142.

Bochenek, W., 2012: Ocena zmian warunków opadowych na Stacji naukowo-badawczej IGIPZ PAN w Szymbarku w okresie 40 lat obserwacji (1971–2010) i ich wpływ na zmienność odpływu wody ze zlewni Bystrzanki. *Water-Environment-Rural Areas 12*, 2(38), 29–44 (in Polish)..

Brunetti, M.; Maugeri, M., and *Nanni, .T,* 2000: Variations of temperature and precipitation in Italy from 1866–1995. *Theor. Appl. Climatol. 65*, 165–174.

Czarnecka, M. and *Nidzgorska-Lencewicz J.,* 2012: Wieloletnia zmienność sezonowych opadów w Polsce, *Water-Environment-Rural areas*, 12, 2 (38), 45–60 (in Polish).

Degirmendžić, J., Kożuchowski, K. and *Żmudzka, E.,* 2004: Changes of air temperature and precipitation in Poland in the period 1951–2000 and their relationship to atmospheric circulation. *Int. J. Climatol.*, 24, 291–310.

Domonkos, P., and *Tar, K.,* 2003: Long-term changes in observed temperature and precipitation series 1901–1998 from Hungary and their relations to larger scale changes, *Theor. Appl. Climatol. 75*, 131–147.

European Environment Agency, 2014. Trends in annual precipitation across Europe. www.eea.europa.eu/data-and-maps/figures/observed-changes-in-annual-precipitation-1961-4.

Førland, E.J., and *Hanssen-Bauer, J.,* 1995: Changes in "normal" precipitation in Norway and the North Atlantic region. In: (Ed.: *Heikinheimo P.*) International conference on past, present and future climate. Proceedings of the SILMU conference held in Helsinki, Finland, 22–25 August. Academy of Finland, Helsinki, 228–232

Hartmann, D.L.; Klein Tank, A.M.G.; Rusticucci, M.; Alexander, L.V., Brönnimann, S., Charabi, Y., Dentener, F.J., Dlugokencky, E.J., Easterling, D.R., Kaplan, A., Soden, B.J., Thorne, M.P.W., and *Zhai, Wild P.M.*, 2013: Observations: Atmosphere and Surface. In: Climate Change 2013: The Physical Science Basis. In (Eds.: *Stocker, T.F., D. Qin, G.-K. Plattner, M. Tignor, S.K. Allen, J. Boschung, A. Nauels, Y. Xia, V. Bex and P.M. Midgley*) Contribution of Working Group I to the Fifth Assessment Report of the Intergovernmental Panel on Climate Change. Cambridge University Press, Cambridge, United Kingdom and New York, NY, USA.

Hirsch, R.M.; Slack, J.R. and *Smith, R.A.*, 1982 Techniques of trend analysis for monthly water quality data. *Water Resour. Res. 18*,107–121.

Kendall, M.G., 1975: Rank Correlation Methods. Charless Griffin, London.

Kirtman, B., Power, S.B., Adedoyin, J.A., Boer, G.J., Bojariu, R., Camilloni, I., Doblas-Reyes, F.J., Fiore, A.M., Kimoto, M., Meehl, G.A., Prather, M., Sarr, A., Schär, C., Sutton, R., van Oldenborgh, G.J., Vecchi, G. and Wang, H.J., 2013:. Near-term climate change: projections and predictability. In (Eds.: *Stocker, T.F., D. Qin, G.-K., Plattner, M., Tignor, S.K., Allen, J., Boschung, A,. Nauels, Y., Xia, V. Bex* and *P.M. Midgley*) Climate Change: The Physical Science Basis. Contribution of Working Group I to the Fifth Assessment Report of the Intergovernmental Panel on Climate Change. Cambridge University Press, Cambridge, United Kingdom and New York, NY, USA.

Klein Tank, A.M.G. and *Können, G.P.*, 2003: Trends in Indices of Daily Temperature and Precipitation Extremes in Europe, 1946–99. *J. Climate 16*, 3665–3681.

Kondracki, J., 2011: Geografia regionalna Polski, PWN, Warszawa, (in Polish).

Kürbis, K.; Mudelsee, M.; Tetzlaff, G. and Brázdil, R., 2009: Trends in extremes of temperature, dew point, and precipitation from long instrumental series from central Europe, *Theor. Appl. Climatol*, 98, 187–195.

Lupikasza, E., 2010: Spatial and temporal variability of extreme precipitation in Poland in the period 1951–2006. *Int. J. Climatol.*, 30: 991–1007.

Moberg, A; Jones, P.D., Lister, D., Walther, A., Brunet, M., Jacobeit, J., Alexander, L.V., Della-Marta, P.M., Luterbacher, J., Yiou, P., Chen, D., Klein Tank A. M. G., Saladie', O., Sigró, J,, Aguilar, E., Alexandersson, H., Almarza, C., Auer, I., Barriendos, M., Begert, M., Bergström, H., Böhm, R., Butler, C. J., Caesar, J, Drebs, A,, Founda, D., Gerstengarbe, F.-W., Micela, G., Maugeri, M., Österle, H., Pandzic, K., Petrakis, M., Srnec, L., Tolasz, R., Tuomenvirta, H., Werner, Peter C., Linderholm, H., Philipp, A., Wanner, H., and *Xoplak, E.*, 2006: Indices for daily temperature and precipitation extremes in Europe analyzed for the period 1901–2000, *J. Geoph. Res. 111*, D22106.

Niedźwiedź, T., and *Twardosz, R., Walanus, A.*, 2009: Long-term variability of precipitation series in east central Europe in relation to circulation patterns, *Theor. Appl. Climatol. 98*, 337–350.

Olechnowicz-Bobrowska, B., 1970: Częstość dni z opadem w Polsce. Instytut Geografii Polskiej Akademii Nauk, *Prace Geograficzne. 86*, PWN, Warszawa. 75 (in Polish).

Podstawczyńska, A., 2007: Dry and wet periods in Łódź in the XXth Century. *Acta Univ. Lodzensis Folia Geog. Physica 8*, 9–25.

Rodrigo, F.S., 2010: Changes in the probability of extreme daily precipitation observed from 1951 to 2002 in the Iberian Peninsula. *Int. J. Climatol. 30*, 1512–1525.

Schönwiese, C.D., and *Rapp, J.*, 1997: Climate Trend Atlas of Europe Based on Observations 1891–1990. Kluwer Academic Publishers, Dordrecht.

Skowera, B., Kopcińska, J., and *Kopeć, B.*, 2014: Changes in thermal and precipitation conditions in Poland in 1971-2010. *Ann. Warsaw Univ. of Life Sci. - SGGW, Land Reclam. 46*, 153–162.

Skowera, B., and Wojkowski, J., 2015: Ciągi dni z opadem w wybranych mezoregionach Polski Południowej w latach 1971–2010. *Acta Agrophisica, 22*, 435–447. (in Polish).

Sobczyk, M., 2009: Statystyka. Podstawy teoretyczne. Przykłady. Zadania. Wyd. UMCS, Lublin. (in Polish).

Tošić, I., Zorn, M., Ortar, J., Unkaševic, M., Gavrilov, M. B., and *Markovic, S. B.*, 2016: Annual and seasonal variability of precipitation and temperatures in Slovenia from 1961 to 2011, *Atmos. Res.*, 168, 220-233.

Twardosz, R., 2000: Wieloletnia zmienność sum dobowych opadów w Krakowie w powiązaniu z sytuacjami synoptycznymi. [W:] Studies in Physical Geography, Red. B. Obrębska-Starklowa, *Prace Geograficzne Instytutu Geografii UJ 105*, 19–71 (in Polish).

Wibig, J. and *Fortuniak, K.*, 1998: The extreme precipitation conditions in Łódź in the period 1931-1995. *Acta Univ. Lodzensis Folia Geog. Physica*, *3*, 241–249.

IDŐJÁRÁS

Quarterly Journal of the Hungarian Meteorological Service
Vol. 120, No. 4, October – December, 2016, pp. 383–394

Potential benefit of the ensemble forecasts in case of heavy convective weather situations

Dóra Lázár[1] and **István Ihász**[2*]

[1]*Department of Meteorology, Eötvös Loránd University,*
P.O. Box 32, H-1518 Budapest, Hungary
E-mail: ldora1989@gmail.com

[2]*Hungarian Meteorological Service,*
H-1675 Budapest, P.O.Box 39.
E-mail: ihasz.i@met.hu

**Corresponding author*

(Manuscript received in final form November 15, 2016)

Abstract— Nowadays, early warning and alarm for high impact weather situations becomes more and more important. Besides deterministic model forecasts, using ensemble forecasts gets increasing attention, but in case of the convective events, probabilistic forecasts have not been widely used. Due to the fact that convective events are very changeable in space and time, probabilistic approach can have a lot of advantages. Current horizontal resolution of the global ensemble models is around 30 km, so we cannot aim to focus on small scale convective events, but focusing on frontal zones and extended squall lines can be possible. We attempt pioneering steps to develop new methods and tools to support early warning based on ensemble (ENS) forecasts of the European Centre for Medium-Range Weather Forecast (ECMWF). We focus on the forecast probabilities of three main components generating convection.

Key-words: convection, convective available potential energy, ensemble timeline diagram, ensemble vertical profile, probability charts, relative humidity, statistical and case studies, wind shear

1. Introduction

Protection of life and property is one of the most important tasks of weather forecasts. Heavy convective events quite often cause heavy rainfall, hail, or extremely strong wind causing severe damages. The European unified warning system, the so-called Meteoalarm collects the alert information coming from

member states of EUMETNET. It provides real time warning on its website: www.meteoalarm.eu. The Hungarian Meteorological Service has been maintaining a warning system for counties and alert system for subregional areas since August 1, 2011. This system provides warnings for up to maximum 48 hours (current day and one day ahead) and alerts for ultra short-range (0.5 – 3 hours). The warning system is mostly based on forecasts coming from different models, for this purpose mainly deterministic models were used in the past. The alert system is mostly based on radar and satellite information besides ultra short-range model forecasts. Even nowadays, usage of the global and regional ensemble models gets increasing attention (*Molteni et al.*, 1996, *Palmer*, 2006; *Persson* and *Riddaway*, 2011, *Barkmeijer et al.*, 2012).

Every five years ECMWF makes a strategic plan covering the forthcoming 10 years. In the current ECMWF's Strategic Plan covering the period 2016–2025, developing methods for early warning up to 4–5 days is among the key elements of the strategy (ECMWF, 2016). During our work, we developed a few new objective methods supporting warnings based on ensemble forecasts.

For the development of heavy convective events, three components are needed: atmospheric vertical instability, adequate moisture, and vertical wind shear (*Horváth* and *Geresdi*, 2001; *Craven* and *Brooks*, 2002).

The atmospheric vertical instability is often characterized by the so-called instability index. One of the most popular and often used indexes is the convective available potential energy (short name is CAPE). CAPE is computed according to the following formula:

$$CAPE = \int_{LFC}^{EL} g \frac{T'_v - T_v}{T_v} dz, \tag{1}$$

where *EL* is the equilibrium level (the height at which a rising parcel of air is at the same temperature as its environment), *LFC* is the level of free convection (the height at which the relative humidity of an air parcel will reach 100% when it is cooled by dry adiabatic lifting), g is the gravity, and T_v is the virtual temperature (the temperature at which a theoretical dry air parcel would have a total pressure and density equal to the moist parcel of air).

Vertical wind shear is also a critical factor in the development of the thunderstorms. Vertical wind shear, or the change of winds with height, interacts dynamically with thunderstorms to either enhance or diminish vertical upwelling. So we used the CAPE index, relative humidity, and vertical wind shear (*Horváth*, 2007).

Focusing on these three meteorological parameters, we examined benefits of the usage of ensemble forecasts. To support this, a comprehensive set of tools has been developed.

Our study provides a summary of the newly developed methods based on ECMWF ensemble forecasts (ENS) to assist successful prediction of the convective weather situations. In the first part of the study, key elements of the new approach are presented and illustrated by a few examples. In the second part, result of the statistical investigation is summarized. In the third part, only one selected case study is presented due to some space constraints. Finally, we summarize the benefits of this new system and we have a short outlook too.

2. Statistical studies

Statistical studies of these three parameters were based on a ten-year period of a 51-member ensemble forecasting model for the convective summer season (*Fig. 1*). Relationships between the rate of the convective and total precipitation and the aforementioned three parameters were studied by different statistical methods. On the histogram of CAPE, the values decreased exponentially. On the histograms of the wind shear and relative humidity, the distributions were lognormal.

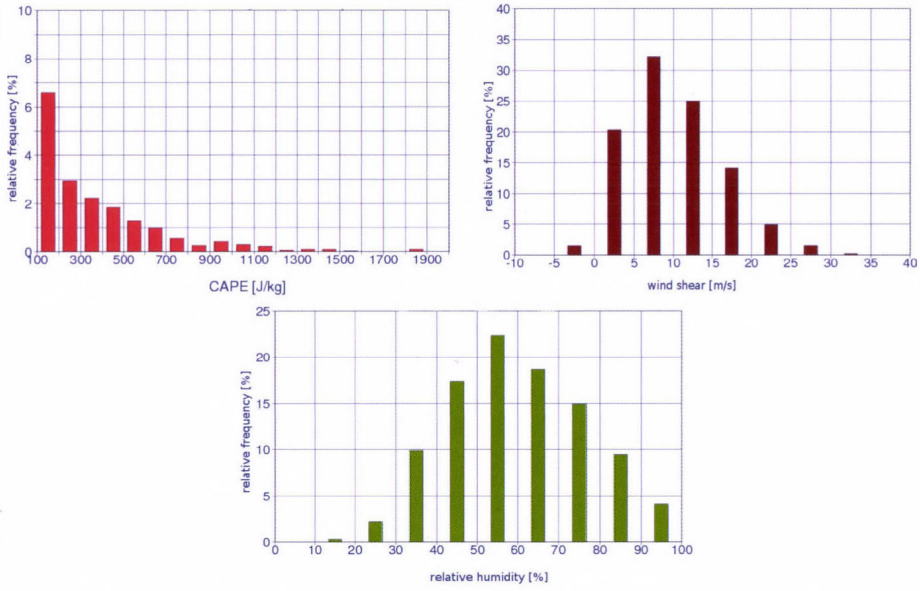

Fig. 1. Histograms of CAPE (J/kg), wind shear (m/s), and relative humidity (%) in summer seasons for Budapest between 2004 and 2013.

We studied whether high rate of convective precipitation was associated with high CAPE values in convective weather situations. Convective/total precipitation rate was calculated and the relationship of these two parameters was studied with crossdiagrams (*Fig. 2*). The thresholds of the CAPE were 0,

500, 1000, 1500, 2000, and 2500 J/kg, and the comparison of the convective/total precipitation rate and CAPE was made for selected thresholds of total precipitation (0, 1, 5, 10, 15, 20, and 25 mm). In the most typical situation, low convective/total precipitation rate was connected with low CAPE values. In case of the extreme values, this relationship was not so strong, thus strong convection was connected not only with CAPE, some other meteorological variables could be quite important too.

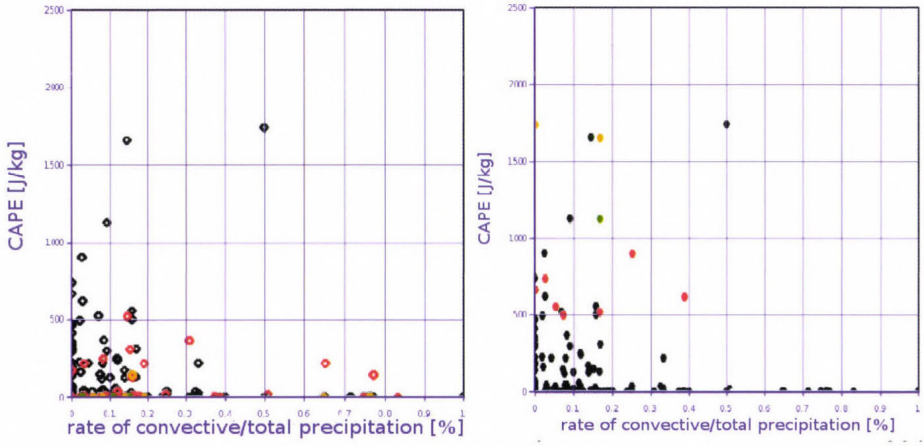

Fig. 2. Crossdiagrams of CP/TP precipitation rate and CAPE values: (left) threshold of CAPE: 0 J/kg, thresholds of precipitation (with quantity): black dot: 0 – 5 mm (125 cases), red dot: 5 – 15 mm (38 cases), orange dot: 15 – 20 mm (3 cases), green dot: above 20 mm (2 cases) for Budapest, (right) threshold of precipitation: 0 mm, thresholds of CAPE (with quantity): black dot: 0 – 500 J/kg (163 cases), red dot: 500 – 1000 J/kg (7 cases), orange dot: 1000 – 1500 J/kg (1 cases), green dot: above 1500 J/kg (1 case) for Budapest

We studied the characteristics of the convective/total precipitation rate forecasts based on different model runs. As the most intensive convective activity typically occurs in the early afternoon, it seemed to be useful to study the similarities and differences of the 00 and 12 UTC model runs. On the histogram *(Fig. 3)*, the total 24-hour sum of the precipitation can be seen, 00 and 12 UTC ENS and control models associated with different thresholds (1, 5, 10, 15, 20, and 25 mm) were plotted. Generally, the 12 UTC model runs produced less number of heavy convective cases than the 00 UTC model runs, but with increasing CP/TP ratio to the proportion of the former grows. At the thresholds of 1 and 5 mm, the relative frequency of the CP/TP ratio extends from 10 to a maximum of 15%. At 15 mm, another column of 75–85% appeared (not shown). At 20 and 25 mm, due to the low number of cases, comparing distributions was not possible.

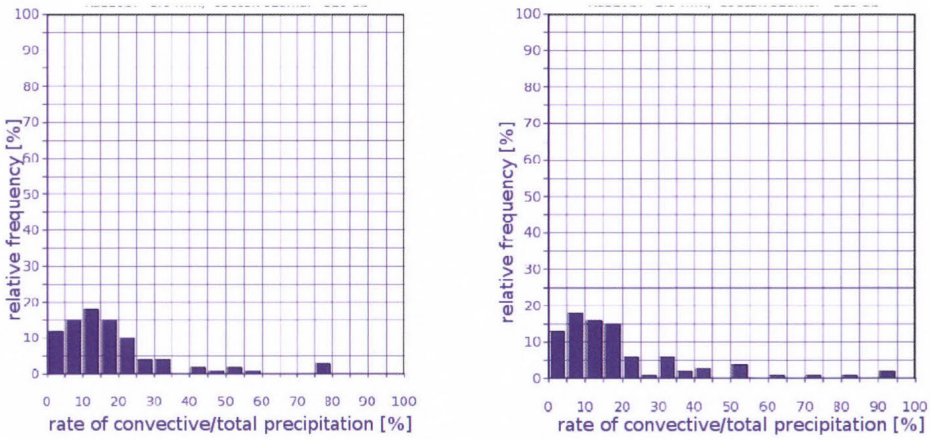

Fig. 3. Histograms for rate of the convective and total precipitation with 1 mm threshold for Budapest: (left) 00 UTC (116 cases), (right) 12 UTC (115 cases)

We also examined the similarity of the distribution curves with the help of the two-sample Kolmogorov-Smirnov test. We checked the condition whether the distribution functions of random examined variable corresponds to a specific distribution function. Consider the (ξ, η) as a random variable pair and ξ, η, n_1 and n_2 as thereof derived independent element patterns. Mark the distribution function of ξ as $F(x)$, the empirical distribution function calculated from the sample as $F_{n1}(x)$, and using the same method for the random variable η, mark its distribution function and empirical distribution function as $G(x)$ and $G_{n2}(x)$. Chosen probe attached to the probe test statistic:

$$D_{1,2} = \sqrt{\frac{n_1 - n_2}{n_1 + n_2}} \left(\sup \left| F_{n_1}(x) - G_{n_2}(x) \right| \right), \tag{2}$$

whereof (*Kolmogorov*, 1933, *Smirnov*, 1936):

$$P\left(D_{1,2} < x\right) = K(x), \tag{3}$$

where $K(x)$ is the limit distribution function. To define the range of acceptance, it is necessary to assign x_α values for the most important levels of significance (*Table 1*).

Table 1. x_α values for the most important levels of significance

A	0.1	0.05	0.001
x_α	1.23	1.36	1.63

We take the x_α values from the table of $K(x)$ distribution function, $K(x_\alpha) = 1-\alpha$. Our acceptance range of $(0, x_\alpha)$ interval is on the level of α significance. Thus, the null hypothesis is kept $0 \leq D_n < x_\alpha$. The null hypothesis is rejected when $D_n \geq x_\alpha$ (*Dévényi* and *Gulyás,* 1988).

As our value was about 2.1, it was found that in a 95% hypothesis test the distribution of the convective/total precipitation rates for 24 hours based on 00 and 12 UTC model runs are different. In both cases of the visual and statistical methods, the same conclusion was made.

In this chapter, three parameters (CAPE, wind shear, relative humidity) were examined with statistical methods which revealed their physical features. Long-period investigations showed the most frequent values and revealed the attributes of the above-mentioned parameters. Using these data in the case studies, the threshold values can be easily chosen. We studied the relationship between the CAPE values and the convective/total precipitation rate, therefore, the convective/total precipitation rate parameter was added to the examination. Thereafter, features of the convective/total precipitation rate were examined with various time and threshold values on histograms and with the Kolmogorov-Smirnov test too.

3. New comprehensive probabilistic approach to forecast convective events

As it has been mentioned, CAPE index, relative humidity, and vertical wind shear were investigated. Focusing on these three meteorological parameters, we studied potential opportunities of the ensemble forecasts with four newly developed graphical tools.

Two of the four visualization methods, the ensemble meteogram and the ensemble vertical profiles (*Ihász* and *Tajti*, 2011) were available at the beginning of our work. These two point forecast products have been operationally available at the Unit of Methodology Development of Hungarian Meteorological Service since 2011. Both methods show probability distributions of the meteorological parameters for the selected location.

On the ensemble meteogram you can see the probability of the CAPE index, the wind shear between 10 m and the 500 hPa level, and the average relative humidity between 850 and 500 hPa levels. The ensemble vertical profile is based on temperature, dew point, wind direction and speed at 91 ensemble model levels.

Additionally, we developed two new methods for studying convective events. The first method provides probability map of the event exceeding predefined thresholds. Probability of CAPE, wind shear, and relative humidity with other parameters are studied. Other parameters are the 500 hPa geopotential height, 300 hPa potential vorticity, and convective precipitation. Applying this approach we can study weather situations in more details. Intensity of the dangerous weather conditions can be well estimated. Intensive convective periods are clearly marked during the forecasting period. Another new visualization tool shows time evolution of predefined multiple thresholds in graphical form for any selected location. In our case studies, CAPE and wind shear with different thresholds were examined.

First of all, our aim was to study the probability maps, so we could identify the time and spatial location of the convective weather situation. Then we used multiple thresholds timeline diagrams in selected points, so we could see when the most extreme values of these parameters were predicted and how they changed in time. In the third part of our study we investigated the evolution of the vertical properties of the atmosphere in time. In the end, we studied the relationships among these three parameters with ensemble meteograms. We studied the day-to-day consistency of the forecasts too, so the analyzed period was between day –4 and day –1 before the event.

Horizontal resolution of the numerical models are regularly increased (*Horányi et al.,* 2011, *Szintai et al.,* 2015). In spring 2016, ECMWF increased the horizontal resolution of the high resolution (deterministic) model from 16 km to 9 km. At the same time, the horizontal resolution of the ensemble model changed from 32 km to 18 km. After 2020 running of global non-hydrostatic models would be necessary (*Wedi* and *Malardel*, 2010). These developments will likely cause increasing reliability of the forecasts in heavy convective situations too.

In this chapter, new applied visualization tools were presented. We intended to explore their applicability in forecast situations, therefore case studies were investigated. A selected case study is presented in the next chapter.

4. Case study of heavy convective events

During our former studies (*Lázár,* 2013), comprehensive case studies were done. Weather situations representing different type of convective events were selected in summer 2012. In this paper, weather situation of July 29, 2013 is presented, this event followed the hottest period of summer 2013. On July 29, 2013 lots of thunderstorms were observed in Hungary (*Horváth* and *Kolhmann*, 2013).

It was a really hot weather situation when new record maximum temperatures were registered before a thunderstorm line reached Hungary. In

front of the cold front, the temperature had been increasing and 23 °C appeared at the 850 hPa level. In Western Europe, intense thunderstorms connected to the cold front were erupted. Around 20 UTC, the upper air cold front with stormy winds (60–80 km/h) reached the Transdanubian Region from southwest direction. In the early hours of July 29, the northwestern cold front arrived in the lowest levels.

During our study, first the probability maps were examined, forecasts of day –4 to day –1 were used (*Fig. 4*). The investigated time was July 29, 2013, 21 UTC, so the studied forecasts were made on the following three consecutive days: July 26, 27, 28, 2013, 00 UTC. High probability of high CAPE values could be seen in the northwestern part of the country. The local maximum of the potential vorticity was located northwest to this area. A pair of ridge and trough was connected to this region too, the latest forecast showed stronger contrast between the ridge and trough.

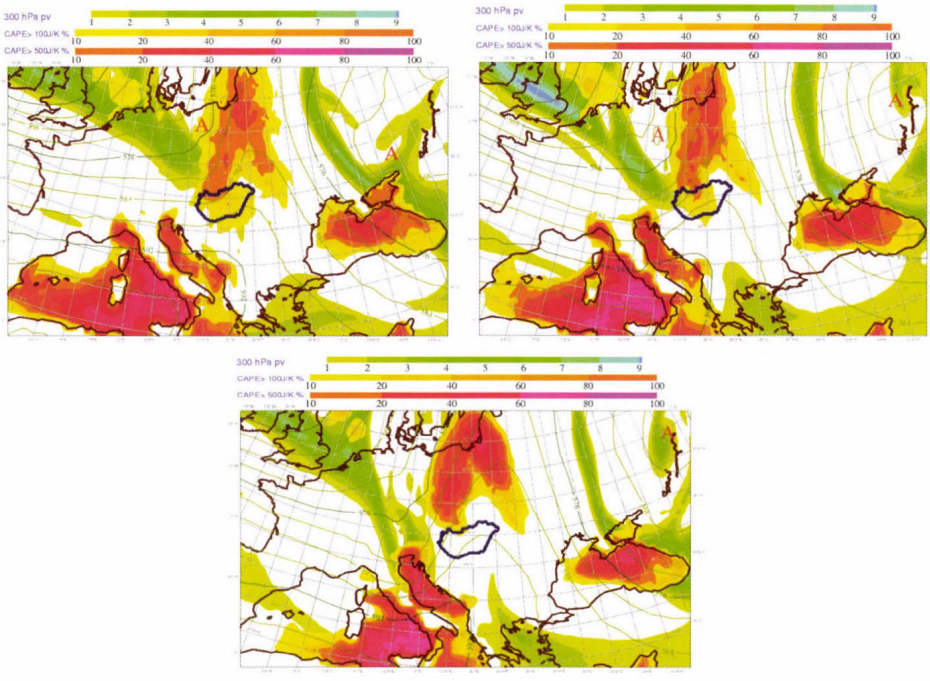

Fig. 4. Forecast of the CAPE probability (shaded yellow to pink), potential vorticity values (shaded green to blue), and 500 hPa height fields (green lines) at July 29, 2013, 21 UTC (by forecast of July 26, 2013, 00 UTC + 93 hours, July 27, 2013, 00 UTC +69 hours, and July 28, 2013, 00 UTC +45 hours)

At the second step, particular locations, like Szombathely were selected, where the time evolution of the predefined multiple thresholds of CAPE values was studied. The most dangerous time period, early late afternoon was predicted in every model run. Intensity of the probabilities was changed from model run to model run (*Fig. 5*).

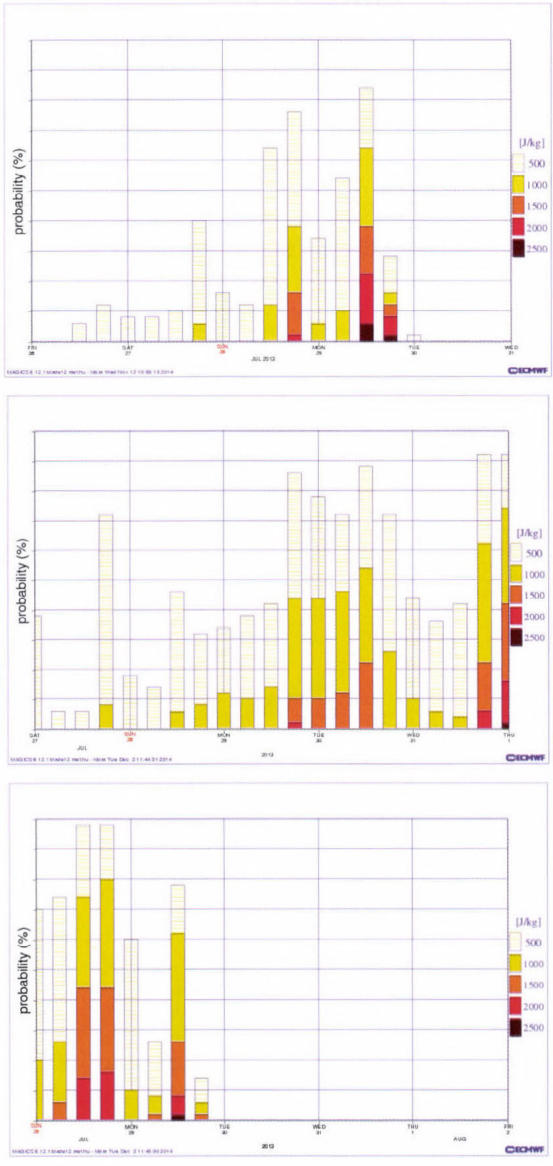

Fig.5. Time evolution of predefined multiple thresholds of CAPE values (the thresholds: 500 (yellow dot), 1000 (yellow), 1500 (orange), 2000 (red) and 2500 (brown) J/kg) based on modeled values of July 26, 27, 28, 2013 for Szombathely.

The third studied diagram was the ensemble vertical profile for the selected location (*Fig. 6*). It can be clearly seen, that the lower troposphere was relatively dry, and between 700 and 300 hPa an extended wet layer could be found which supported the possibility of severe convective events.

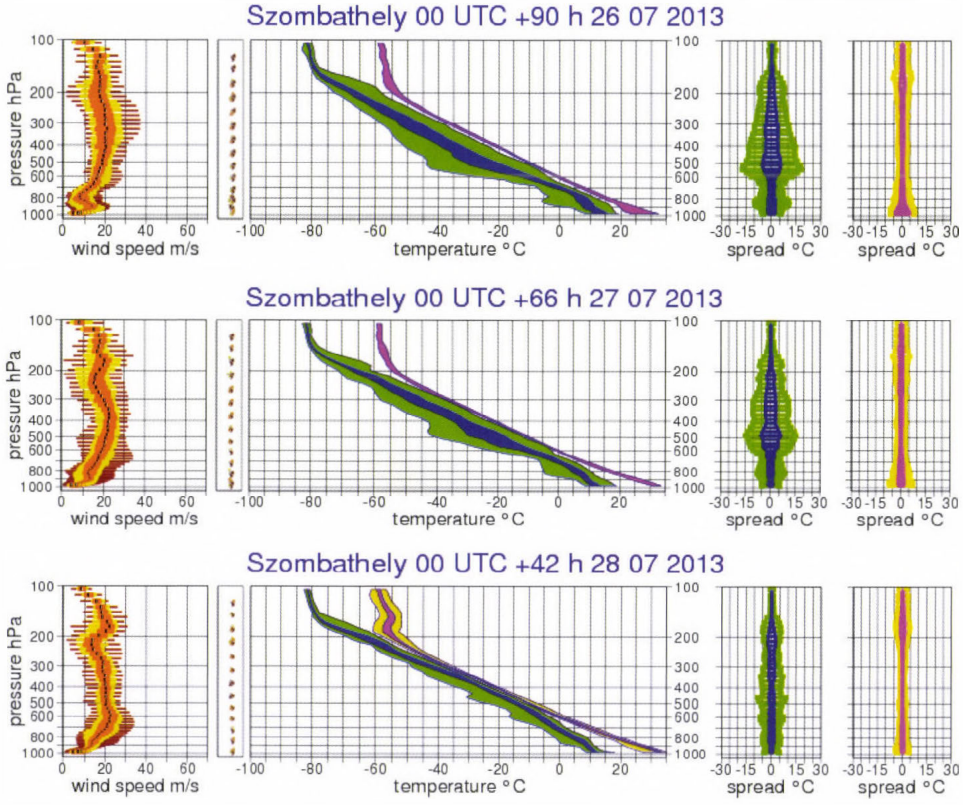

Fig. 6. Ensemble vertical profiles based on model runs of 00 UTC July 26, 27, 28, 2013 for Szombathely

Finally, we studied the ensemble meteograms of these three parameters (*Fig. 7*). In the forecast of July 27, 00 UTC, it could be seen that the probabilities of the CAPE and wind shear were increasing gradually until the evening of July 29. Probabilities of the relative humidity were decreasing gradually until the evening of July 29. After July 30, the CAPE values were near to zero, the intensity of the wind shear decreased, and the relative humidity increased. This statement could be seen in the forecast of July 28, 00 UTC, but it was not so much strong as in the forecast of July 27, 00 UTC.

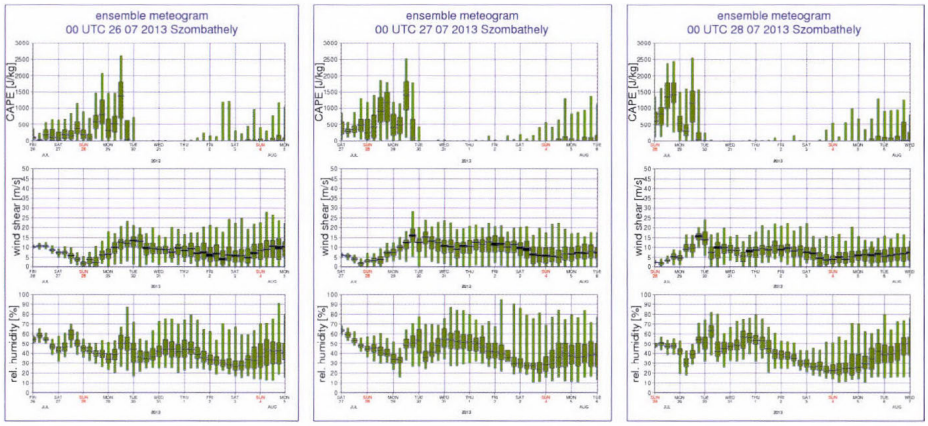

Fig. 7. Ensemble meteograms of CAPE (top), wind shear (middle), relative humidity (bottom) of July 26, 27, 28, 2013 for Szombathely.

5. Summary and conclusions

In this paper, it was shown how important it is to forecast the probability of the dangerous weather situations as precisely as possible. We attempted to provide a combination of new probabilistic tools for supporting successful forecasts of dangerous weather situations. Four graphical probabilistic methods were applied for three meteorological parameters, which are CAPE, wind shear, and relative humidity. It can be stated that wind shear is the most predictable parameter. Relative humidity has more uncertainty, but mostly it can be characterized as a respectable parameter. The medium-term forecast of CAPE index is not always successful, but with other fields it can provide useful extra information in the operational forecast. In the future, this new complex approach can be used for high resolution hydrostatic and nonhydrostatic ensemble models, as ALADIN and AROME.

References

Barkmeijer, J, Buizza, R., Kallen, E., Molteni, E., Mureau, R., Palmer, T., Tibaldi, S., and *Tribia, J.,* 2012: 20 years of ensemble prediction at ECMWF. *ECMWF Newsletter 134*, 16–32.

Craven, J.P. and *Brooks, H.E*, 2002: Baseline climatology of sounding derived parameters associated with deep moist convection. Proceeding of The 21st Conference on Severe Local Storms and 19th Conference on Weather Analysis and Forecasting/15th Conference on Numerical Weather Prediction. San Antonio, TX, 11-16 August 2002.

ECMWF, 2016: The ECMWF Strategy, 2016-2025, Reading, United Kingdom, 13.

Dévényi, D. and *Gulyás, O.*, 1988: Matematikai statisztikai módszerek a meteorológiában. Tankönyvkiadó, Budapest, 235-236. (in Hungarian)

Horányi, A., Mile, M., and *Szűcs, M.,* 2011: Latest developments around the ALADIN operational short-range ensemble prediction system in Hungary, *Tellus 63A*, 642–651.

Horváth, Á. and *Geresdi, I.*, 2001: Severe convective storms and associated phenomena in Hungary. *Atmos. Res. 56*, 127–146.

Horváth, Á., 2007: The ingredients of atmospheric convection. *In A légköri konvekció.* Hungarian Meteorological Service. Budapest, 4–17. (in Hungarian)

Horváth, Á. and *Kohlmann, M.*, 2013: Egy forró periódus vége. Hungarian Meteorological Service. July 31. 2013. (http://www.met.hu). (in Hungarian)

Ihász, I. and Tajti, D., 2011: Use of ECMWF's ensemble vertical profiles at the Hungarian Meteorological Service. *ECMWF Newsletter 129,* 25–29.

Kolmogorov, A.N., 1933: Sulla determininazione empirica di una legge, *Giornale dell' Instituto Italiano degli Attuari 4*, 83–91. (in Italian)

Molteni, F.R., Buizza, T.N., Palmer, T.N., and *Petroliagis*, 1996: The ECMWF ensemble prediction system: methodology and validation. *Q.J.Roy. Meteorol. Soc. 122*, 37–119.

Smirnov, N.V., 1936: Sui la distribution w2 (Criterium de M.R.v Mises), *Comptes Rendus*, Paris, 202, pp. 449-452. (in French)

Palmer, T.N., 2006, Predictability of Weather and Climate from theory to practice. In (*Eds.: Palmer, T.N. and Hagedorn, R.*) Predictability of Weather and Climate, Palmer and Hagedorn, Cambridge Univ, Press, 1–29.

Persson, A. and *Riddaway, B.*, 2011: Increasing trust in medium-range weather forecasts. *ECMWF Newsletter 129,* 8–12.

Lázár, D., 2012: Valószínűségi előrejelzések alkalmazhatósága a nyári konvektív időjárási helyzetekben. Master Thesis, Eötvös Loránd University, Budapest. (in Hungarian)

Szintai, B., Szűcs, M., Randriamampianina, R., and *Kullmann, L.*, 2015: Application of the AROME non-hydrostatic model at the Hungarian Meteorological Service: physical parameterizations and ensemble forecasting. *Időjárás 119*, 215–241.

Wedi, N. and *Malardel, S.*, 2010: Non-hydrostatic modelling at ECMWF. *ECMWF Newsletter 125,* 17–21.

IDŐJÁRÁS

Quarterly Journal of the Hungarian Meteorological Service
Vol. 120, No. 4, October – December, 2016, pp. 395–414

Impact of atmospheric circulation on the occurrence of heat waves in southeastern Europe

Arkadiusz M. Tomczyk

Department of Climatology, Adam Mickiewicz University in Poznań,
Dzięlgielowa 27, 61-680 Poznań, Poland
E-mail: atomczyk@amu.edu.pl

(Manuscript received in final form May 31, 2016)

Abstract—The main objective of this article is to identify the pressure conditions conducive to the occurrence of heat waves in southeastern Europe. Before this objective could be achieved, the spatial and temporal variability of the occurrence of heat waves in the region were determined. This article defines a hot day as a day of maximum temperature (Tmax) above the 95th annual percentile, and a heat wave is considered to be a sequence of at least 5 such days. The study is based on the data of 21 stations from the period 1973–2010. In the discussed period, at all stations, a statistically significant increase in Tmax and the number of hot days were observed. The total number of heat waves fluctuated from 25 in Burgas to 48 in Drobeta-Turnu Severin, Skopje, and Split, while the sum durations of heat waves ranged between 173 days in Botosani and 414 in Split. Heat waves in southeastern Europe occurred most often when a ridge of high pressure lay over Europe. This system caused the inflow of continental air masses from the northeast or east. An alternative source of air masses causing heat waves was advection from the south.

Key-words: heat waves, atmospheric circulation, climate change, southeastern Europe

1. Introduction

One of the most important factors determining weather and climate conditions is atmospheric circulation (*Chromow,* 1952; *Niedźwiedź,* 1981; *Yarnal,* 1993). In particular, high pressure systems and blocking situations, which determine the meteorological conditions of a particular region by breaking zonal circulation, are of great importance (*Bielec-Bąkowska,* 2014). The consequence of such patterns is the occurrence of heat waves in summer and frost waves in winter

(*Porębska* and *Zdunek,* 2013; *Bielec-Bąkowska,* 2014). The impact of atmospheric circulation on thermal conditions and the occurrence of thermal extremes has been the subject of many studies (*Founda* and *Giannakopoulos,* 2009; *Avotniece et al.,* 2010; *Ustrnul et al.,* 2010; *Kažys et al.,* 2011; *Porębska* and *Zdunek,* 2013; *Tomczyk* and *Bednorz,* 2014; *Unkašević* and *Tošić,* 2015; *Tomczyk* and *Bednorz,* 2016). Further and more detailed research is required into the importance of circulation, and above all its changes, both global and local, as well as from both a holistic perspective and a perspective taking its particular elements into consideration (*Bielec-Bąkowska,* 2014).

According to the authors of the Fifth IPCC Assessment Report (2013), in each of the last three decades, at the Earth's surface temperature was higher than in the preceding decade and, simultaneously, higher than in any previous decade since 1850; in the Northern Hemisphere, the period of 1983–2012 was probably the warmest 30-year period in the last 1400 years. One manifestation of the observed warming is the increasing frequency of extremely hot days and heat waves (*Avotniece et al.,* 2010; *Kyselý,* 2010; *Shevchenko et al.,* 2014; *Keggenhoff et al.,* 2015; *Unkašević* and *Tošić,* 2015; *Tomczyk* and *Bednorz,* 2016; *Tomczyk et al.,* 2016), with the simultaneous decrease in frost days and frost waves (*Kejna et al.,* 2009; *Avotniece et al.,* 2010; *Bednorz,* 2011; *Mužíková et al.* 2011; *Niedźwiedź et al.,* 2012; *Krzyżewska,* 2014; *Migała et al.,* 2016). The heat waves from 2003 to 2010, defined as "mega heat waves," caused more than 500-year records for seasonal air temperatures across approximately 50% of the area of Europe (*Barriopedro et al.,* 2011).

In recent years, there has been an increase in the number of publications concerning extreme weather phenomena, including heat waves. These publications have largely focused on determining the influence of heat waves on the number of deaths caused by biometeorological conditions affecting human body systems (*Johnson et al.,* 2005; *Poumadere et al.,* 2005; *Paldy* and *Bobvos,* 2009; *Shaposhnikov et al.,* 2014; *Bobvos et al.,* 2015; *Revich et al.,* 2015). Despite these numerous scientific works, there is still a noticeable deficiency of scientific papers analyzing the occurrence of heat waves on the basis of long and uniform data series for the different regions of Europe. Therefore, the objective of this article was to determine the spatial and temporal variability of the occurrence of heat waves in southeastern Europe. However, the main emphasis of this article was to identify the atmospheric conditions conducive to the occurrence of heat waves in this part of Europe. The undertaking of this subject is especially relevant in light of forecasts which show that heat waves in the 21st century are going to be not only more frequent, but also longer and more intensive (*Meehl* and *Tebaldi,* 2004; *Beniston et al.,* 2007; *Koffi* and *Koffi,* 2008; *Kürbis et. al.,* 2009; *Kyselý,* 2010; *Pongracz et al.,* 2013; *Zacharias et al.,* 2015).

2. *Methods and data*

This article used daily values of the maximum (Tmax), minimum (Tmin), and mean air temperature (T) for 21 stations located in eight countries: Bulgaria, Croatia, Greece, Macedonia, Romania, Serbia, Slovenia, and Hungary (*Fig. 1*). The article defined this area simply as southeastern Europe. The data were obtained for the period of 1973–2010 from the freely accessible databases of the National Oceanic and Atmospheric Administration (NOAA).

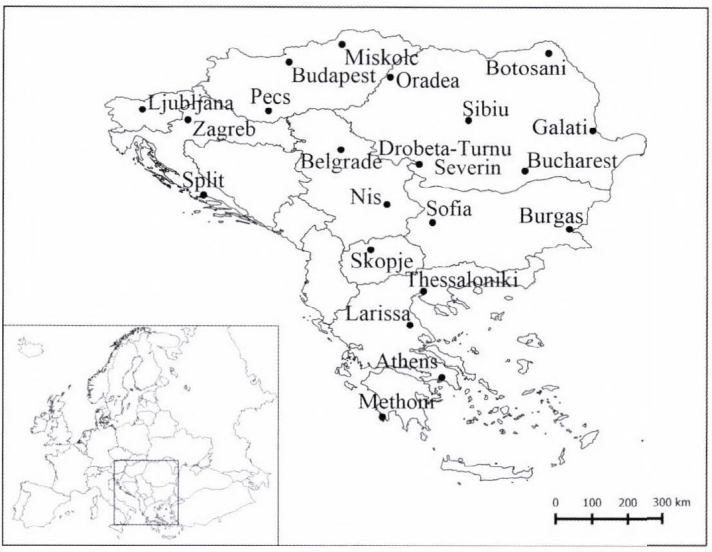

Fig. 1. Locations of the meteorological stations.

This article defines a hot day as a day with Tmax above the 95th annual percentile (*Fig. 2a*), and a heat wave (HW) is considered to be a sequence of at least 5 hot days. This assumption is based on the definition of an extreme weather event included in the IPCC reports (2007), according to which, a weather phenomenon is defined as an extreme weather event if it is so rare within a particular area and in a particular season that it lies within the range of the 10th or 90th percentile of an observed probability density function, or rarer. This definition of a HW has been used in articles concerning, among others, the occurrence of HWs in central Europe (*Tomczyk* and *Bednorz,* 2016) and northern Europe (*Tomczyk et al.,* 2016).

The literature offers equal definitions of HWs which differ in methodological assumptions. According to *Krzyżewska* (2010), this results from the fact that distinguishing HWs is most of all dependent on local climatic conditions, which change with latitude, height above sea level, and direction of air mass inflow. HWs are defined as, among others: (1) a several-day period with the maximum or mean daily temperature above a specific threshold value (*Kyselý,* 2002; *Kosowska-Cezak,* 2010; *Bobvos et al.,* 2015); (2) a period with apparent temperature (AT) above the 95th percentile which starts with a minimum 2.0°C increase in relation to the preceding day (*Kuchcik* and *Degórski,* 2009); (3) a period >5 consecutive days with Tmax >5 °C above the 1961–1990 daily Tmax norm (*Frich et al.,* 2002; *Unkašević* and *Tošić,* 2009).

On the basis of the data, the mean Tmax of the particular months and summer seasons (June–August) was calculated, and hot days were selected to distinguish HWs. Additionally, Pearson's correlation coefficient was calculated between the mean Tmax in summer and the number of hot days. Subsequently, variability within the multiannual period and statistical significance ($p \leq 0.05$) were determined for the distinguished climatological characteristics.

In order to define pressure conditions conducive to the occurrence of HWs, daily values of atmospheric pressure at sea level (SLP), the height of the isobaric surface 500 hPa (z500 hPa), and the temperature on the isobaric surface 850 hPa (T850) were used. The data were obtained from the records of the National Center for Environmental Prediction/National Center for Atmospheric Research (NCEP/NCAR) Reanalysis (*Kalnay et al.,* 1996), which are available in Climate Research Unit resources. In the study, values of SLP and z500 hPa in 120 geographical grid points 2.5°×2.5° for the area of 25°–75°N latitude, 35°W–65°E longitude were used. On the basis of the above-mentioned data, the SLP, z500 hPa, and T850 maps for the summer season (June–August), as well as a collective map for hot days forming HWs were drawn up. The description was supplemented with the drawing up of maps of anomalies. Anomalies were calculated as differences between the mean SLP, z500 hPa, and T850 values for HWs and the mean summer values of these characteristics in the analyzed multiannual period. Only days on which the temperature met the criterion of a hot day in at least five stations were selected for analysis. The circulation types which cause the occurrence of HWs were distinguished by clustering days according to their values of sea-level pressure, using the minimum variance method known as Ward's method (1963). This method is based on Euclidean distances, and in essence involves merging the pair of clusters A and B which, after merging, provide the minimum sum of squares of all objects' deviations from the newly-created cluster's centre of gravity (*Ward,* 1963; *Wilks,* 1995). In order to achieve that, standardized SLP values were used. The standardization was made to deseasonalize the observations, while keeping the intensity of pressure field (*Esteban et al.,* 2005). Clustering methods (among others, Ward's method) are often applied in climatology, e.g., in distinguishing seasons and

climatic regions, and identifying weather types (*Bednorz,* 2008; *Tomczyk* and *Bednorz,* 2016). The maps of SLP, z500 hPa, and T850, as well as maps of anomalies were drawn up for the identified circulation types. Additionally, for the selected days in the distinguished circulation types, there were 48-hour back trajectories of air particles traced by means of the NOAA HYSPLIT model (http://ready.arl.noaa.gov/HYSPLIT.php). Back trajectory analysis enables one to determine the area of origin of air masses on selected days, which constitutes a supplement to the information displayed by weather maps.

3. Results

3.1. Maximum temperature in the summer

In southeastern Europe, between 1973 and 2010, the mean Tmax in summer was 27.8 °C and ranged from 25.0 °C in Ljubljana to 32.4 °C in Larissa (*Fig. 2b*). In the analyzed period, at all stations the lowest mean Tmax was recorded for the years 1973–1980, and varied then from 23.6 °C in Sibiu to 31.8 °C in Larissa. Meanwhile, in 90% of the stations the highest mean Tmax was observed for the years 2001–2010, and ranged from 25.7 °C in Ljubljana to 33.0 °C in Larissa. Analysing the particular summer seasons, at 67% of the stations, the coldest summer season occurred in 1976, and at 24% of the stations it was in 1978. On the other hand, the warmest season at 52% of the stations was recorded in 2007, and at 43% of them in 2003. Deviation of the mean Tmax in the particular seasons from the mean for the analyzed multiannual period ranged from –4.1 °C in 1976 (Sofia, Skopje) to 4.5 °C in 2007 (Galati). The course of the mean Tmax in the analyzed years shows considerable year-to-year fluctuations. Within the majority of the area, the variability of the mean Tmax was similar, which is proven by its barely-diversified standard deviation values, falling within a range of 0.9–1.5 at 86% of stations. In the analyzed period, at all stations, a statistically significant increase in Tmax in summer was observed. These changes ranged from 0.4 °C/10 years in Thessaloniki to 1.2 °C/10 years in Sofia and Niš (*Fig. 2c*). The aforementioned changes were considerably influenced by an increase in Tmax in the first decade of the 21st century, when Tmax generally exceeded the norm for the 1973–2010 multiannual period. In summer, the highest increase in Tmax was observed in August and, on average, it was 0.9°C/10 years for the analyzed area. In that month, the highest increase was recorded in Sofia, and it was 1.5 °C/10 years.

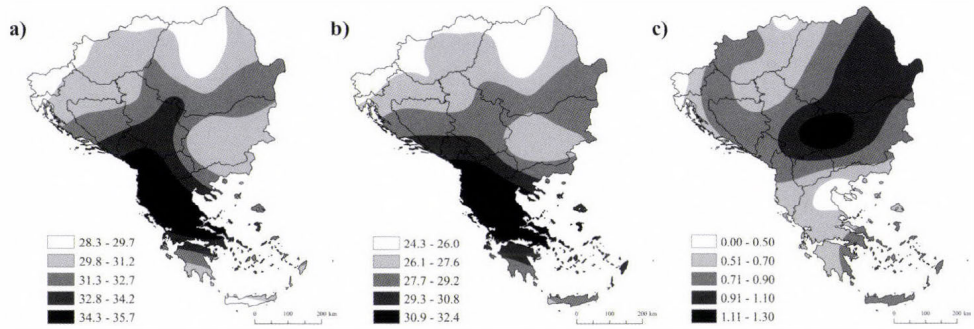

Fig. 2. The value of the 95th annual percentile of the Tmax (°C) (a); the mean Tmax (°C) in the summer (June–August) (b); and changes in the mean summer Tmax in °C/10 years during the period 1973-2010 (c).

3.2. Hot days

In southeastern Europe, the observed increase in Tmax translated into an increase in the number of hot days and, consequently, into an increase in the frequency of occurrence of HWs. At all stations, the coefficient of correlation between the mean Tmax in summer and the number of hot days fluctuated around 0.84–0.93. The average number of hot days in the summer season in the analyzed area was 18. At 95% of the stations, the lowest number of days of the aforementioned category was recorded in the 1973–1980 multiannual period, and their average number ranged from 4 days in Niš to 14 days in Thessaloniki. On the other hand, at 90% of the stations the highest number of hot days occurred in the first decade of the 21st century—then, the average number of hot days varied from 18 days in Oradea to 30 days in Bucharest and Split. When analyzing the particular summer seasons, it was found that at 80% of the stations, the lowest number of hot days—or even zero hot days—were recorded in 1976 or 1978. On the other hand, the highest number of days of the analyzed category was specific for 2003 and 2007, at 33% and 29% of the stations, respectively. In the analyzed period, the maximum number of the days recorded in one year was 57, and it was observed in 2003 in Zagreb and Methoni (*Fig. 3*). In the analyzed period, in southeastern Europe, there was an average increase in observed hot days, which was 6.2 days per 10 years, and it was statistically significant. This increase was not uniform across the analyzed area; changes ranged from 3.5 days/10 years in Miskolc and Larissa, to 8.4 days/10 years in Bucharest, and were statistically significant in all stations (*Fig. 3*). Hot days were recorded from April to November; still, the highest number of those days occurred in July and August, with 38.6% and 38.2% of all hot days,

respectively. At 57% of the stations, the highest number of the above-mentioned days was found in July, while at the rest of the stations it was August. The earliest occurrence of a hot day was as early as 6 April (1998, Bucharest, Galati), and the latest one was November 5 (1980, Methoni); therefore, for the whole analyzed area, the potential period of the occurrence of hot days was 214 days.

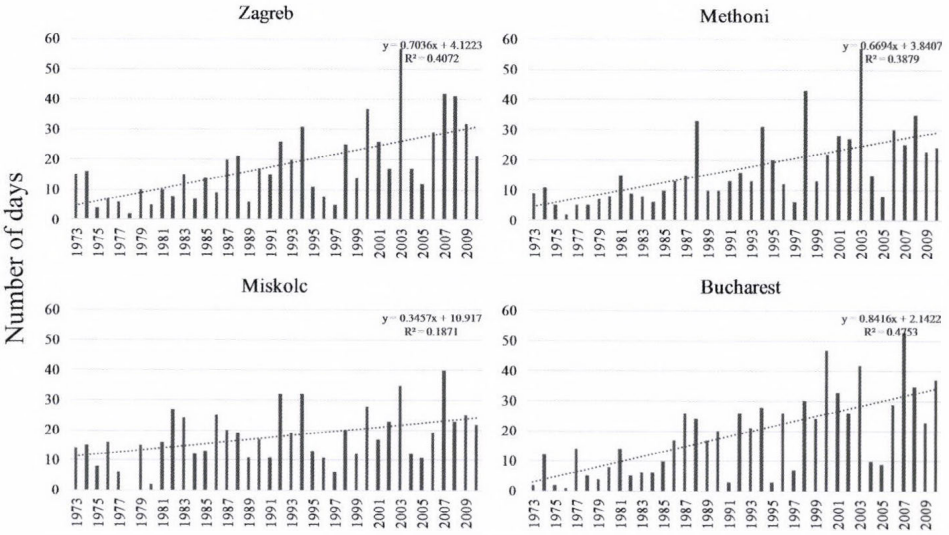

Fig. 3. Multi–year series of the annual number of hot days with the trend line and regression equation at selected stations.

3.3. Heat waves

In southeastern Europe, in the analyzed multiannual period, the total number of HWs ranged from 25 in Burgas to 48 in Drobeta-Turnu Severin, Skopje, and Split. On the other hand, the total duration of HWs ranged from 173 days in Botosani to 414 in Split. In 90% of stations, the fewest—or even zero—HWs were recorded between 1973 and 1980. Within this period, there were no HWs observed in four stations (that is, Botosani, Burgas, Galati, and Methoni), whereas the most waves were observed in Thessaloniki (seven waves), and their total duration was 39 days (*Fig. 4*). On the other hand, at 62% of the stations, the highest number of HWs was recorded between 2001 and 2010. At that multiannual period, the number varied between 7 (Oradea) and 23 (Split). In

14% of stations, the same number of waves was found both in the 1991–2000 period and the 2001–2010 period; still, in the first decade of the 21st century the waves were longer.

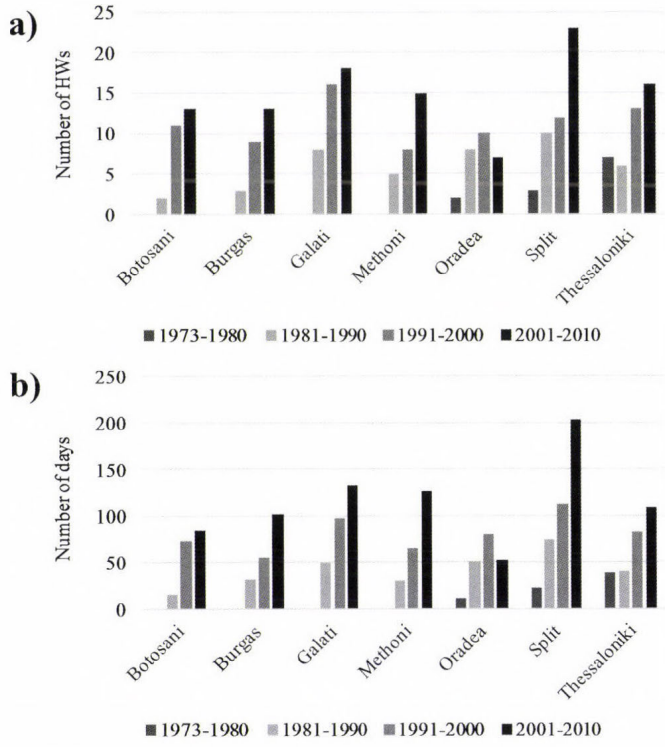

Fig. 4. The number of HWs (a) and the duration of HWs (b) in 1973–2010 at selected stations.

In the analyzed multiannual period in southeastern Europe, HWs occurred from May to September. At 62% of the stations, the highest number of HWs was recorded in August; in the case of two stations, the same number of waves was found in July and August. May HWs (four cases) only occurred in the last decade of the analyzed multiannual period. The earliest HW was recorded in Sibiu on May 7–13, 2003, while the latest, in Sofia and Skopje, were recorded on September 7–15, 1994 and September 9–15, 1994, respectively. The above-mentioned data show that the potential period of the occurrence of HWs within the particular area was 133 days, from May 7 to September 15. In the particular

stations, the duration of this period ranged from 64 days in Burgas (from June 22 to August 24) to 125 days in Sibiu (from May 7 to September 8).

At 81% of the stations, the most HWs were 5-day-long, while at 9% of the stations, there were 6-day waves. 7-day waves were most numerous only in Botosani. Meanwhile, in Sofia, 5- and 6-day waves had a similar frequency. Apart from three stations (Botosani, Burgas, Split), 5- and 6-day waves constituted over 50% of all the recorded waves, and at three stations (Belgrade, Miskolc, Niš), they even constituted over 70%. The longest HW was observed in Methoni, and lasted as long as 38 days, from July 28 to September 3, 2003.

The mean Tmax during the analyzed HWs was 34 °C, while Tmin was 18.8 °C. The highest average Tmax was observed during HWs in Larissa (July 3–9, 2000) and was 40.6 °C. Moreover, at that station, there were four HWs found with a mean Tmax above 40 °C; namely, in 1982, 1987, 1998, and 2007 (*Table 1*). HWs with a mean Tmax above 40 °C were also observed in Niš and Skopje. On the other hand, the highest mean Tmin was found in Athens (July 5–10, 1988), and was 27.1 °C, while the lowest was in Ljubljana (13–17 August 1993) with an average of only 10.7 °C. In the analyzed multiannual period, a statistically significant increase in Tmax during HWs was found at only two stations, while in the case of Tmin, these changes were recorded at seven stations.

Table 1. Occurrence of heat waves with a mean Tmax above 40 °C (their duration and average Tmax) in southeastern Europe between 1973 and 2010

Station	Date	Tmax
Larissa	July 3–9, 2000	40.6 °C
	June 24–28, 1982	40.4 °C
	July 18–27, 1987	40.3 °C
	June 30–July 4, 1998	40.1 °C
	June 19–28, 2007	40.1 °C
Niš	July 15–24, 2007	40.2 °C
Skopje	July 18–26, 1987	40.1 °C

3.4. Impact of circulation on the occurrence of heat waves

The occurrence of HWs (424 days) in southeastern Europe in the analyzed period was connected, on average, with an extensive ridge of high pressure lying across the continent and reaching as far as eastern Europe. Over the analyzed area, SLP ranged from approximately 1008 to 1016 hPa (*Fig. 5a*). Apart from

the northwestern and southern part of the analyzed area, positive anomalies up to > 1 hPa were recorded in the east (*Fig. 5b*). The described system caused an inflow of air masses from the northeast and east. Contour lines of the isobaric surface 500 hPa over southeastern Europe bent northeastward, creating its elevation over the analyzed area, which confirms the settling of warm air masses over this part of the continent. The pattern of z500 hPa contour lines shows western and southwestern air flow in the middle troposphere layer. The described conditions were accompanied by T850 positive anomalies, which fluctuated from 2 to >4 °C over the analyzed area (*Fig. 5c*).

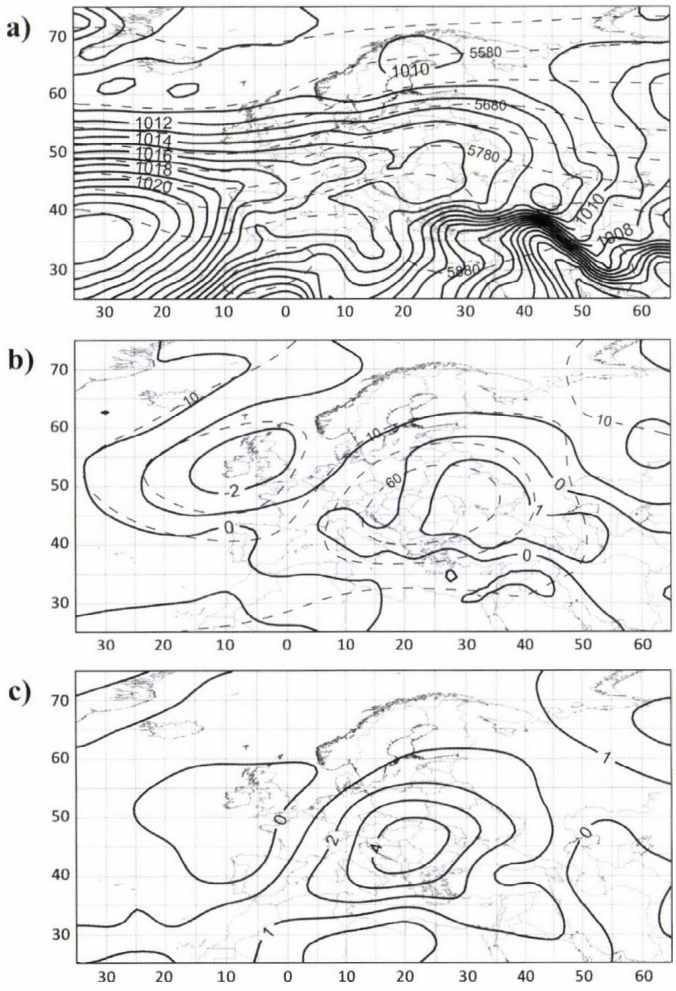

Fig. 5. SLP and z500 hPa (a), SLP and z500 hPa anomalies (b), and anomalies of T850 (c) for the HWs days.

The above-mentioned maps only display pressure conditions which cause the occurrence of HWs in southeastern Europe. However, individual HWs might be caused by different synoptic situations; therefore, the next step consisted in clustering HWs days by SLP, in order to distinguish circulation types. On this basis, two circulation types conducive to the occurrence of HWs within the analyzed area were distinguished. 324 hot days were classified as type 1. On those days, there was a ridge of high pressure settled over Europe, within which, there was a local high-pressure area (>1017 hPa) over the eastern part of the analyzed area (*Fig. 6a*). SLP positive anomalies occurred over the majority of the continent. Over the analyzed area, SLP was higher than the summer average, from approximately 0 to over 2 hPa in the east (*Fig. 6b*). The centre of anomalies was located over central Ukraine, and these exceeded 3 hPa. The described conditions were accompanied by z500 hPa positive anomalies, which fluctuated from 20 to over 90 gpm over southeastern Europe. The presence of warm air masses is also confirmed by T850 positive anomalies, which were from 1 to >4 °C over this part of the continent (*Fig. 6c*). The described system caused an inflow of dry, continental air masses from the northeast and east. This direction of air inflow was also shown by the traced 48-hour back trajectories of air particles for the selected days of this type (*Fig. 7*). All the trajectories showed settlement of air masses, which is typical of high pressure systems.

There were 100 days classified as type 2. The composite maps drawn up for these days show two main pressure systems over Europe, that is, a well-developed Azores High and a low with its centre over southern Scandinavia and Denmark (*Fig. 8a*). A weak pressure gradient occurred over the analyzed area. SLP negative anomalies were recorded over the continent, which ranged between –5 and –2 hPa over the analyzed area (*Fig 8b*). The presence of warm air masses was confirmed by z500 hPa positive anomalies. The settling air masses were warmer than in type 1, which is shown by T850 anomalies. The temperature on the isobaric surface 850 hPa was higher than the summer average by 1 to >6 °C (*Fig. 8c*). The described system caused an inflow of air masses from the southwest, from over northern Africa. This direction of air mass advection was confirmed by the traced back trajectories of air particles (*Fig. 9*). Most of the trajectories show rising air masses, which is typical for low-pressure systems.

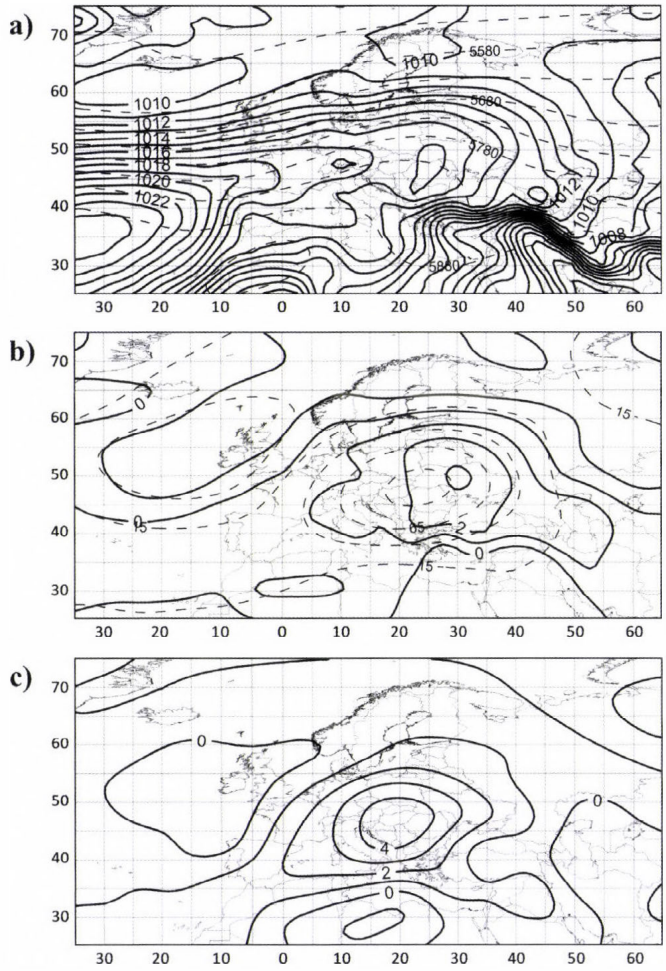

Fig. 6. Mean SLP and z500 hPa (a), SLP and z500 hPa anomalies (b), and anomalies of T850 (c) for the synoptic type 1 causing HWs.

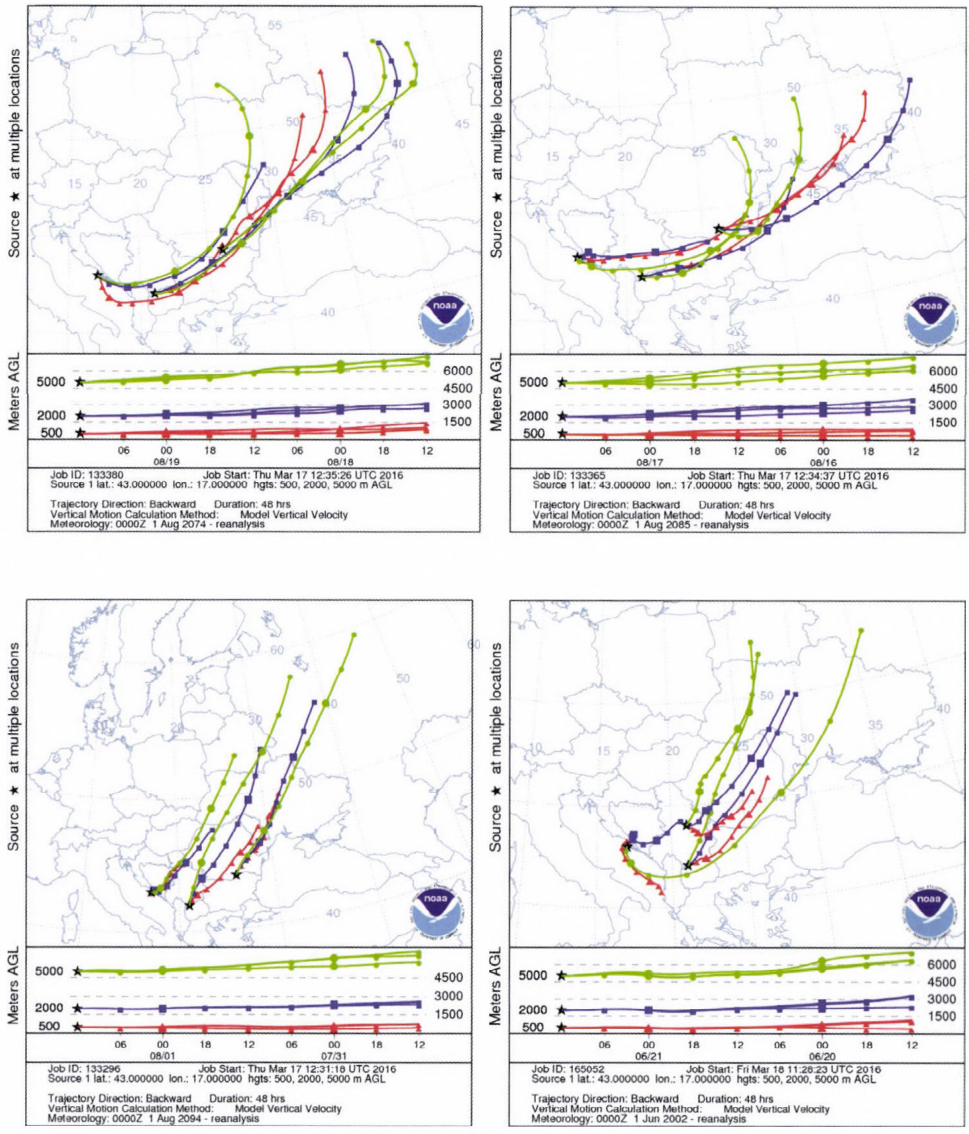

Fig. 7. 48-hour backward trajectories for the selected days in the synoptic type 1 causing HWs based on the reanalyses of the NOAA HYSPLIT model.

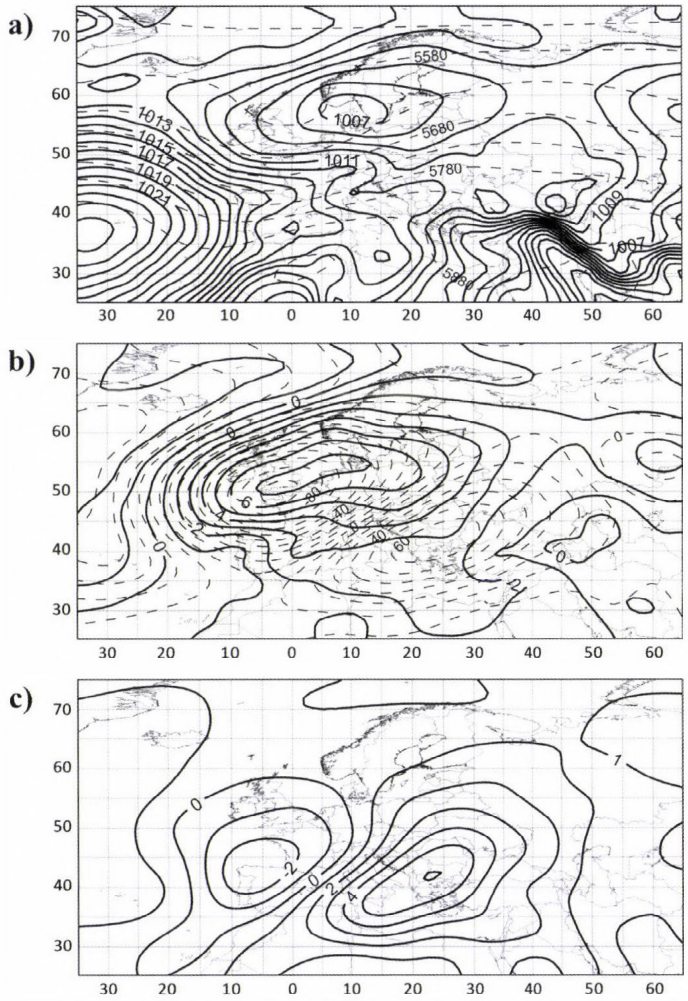

Fig. 8. Mean SLP and z500 hPa (a), SLP and z500 hPa anomalies (b), and anomalies of T850 (c) for the synoptic type 2 causing HWs.

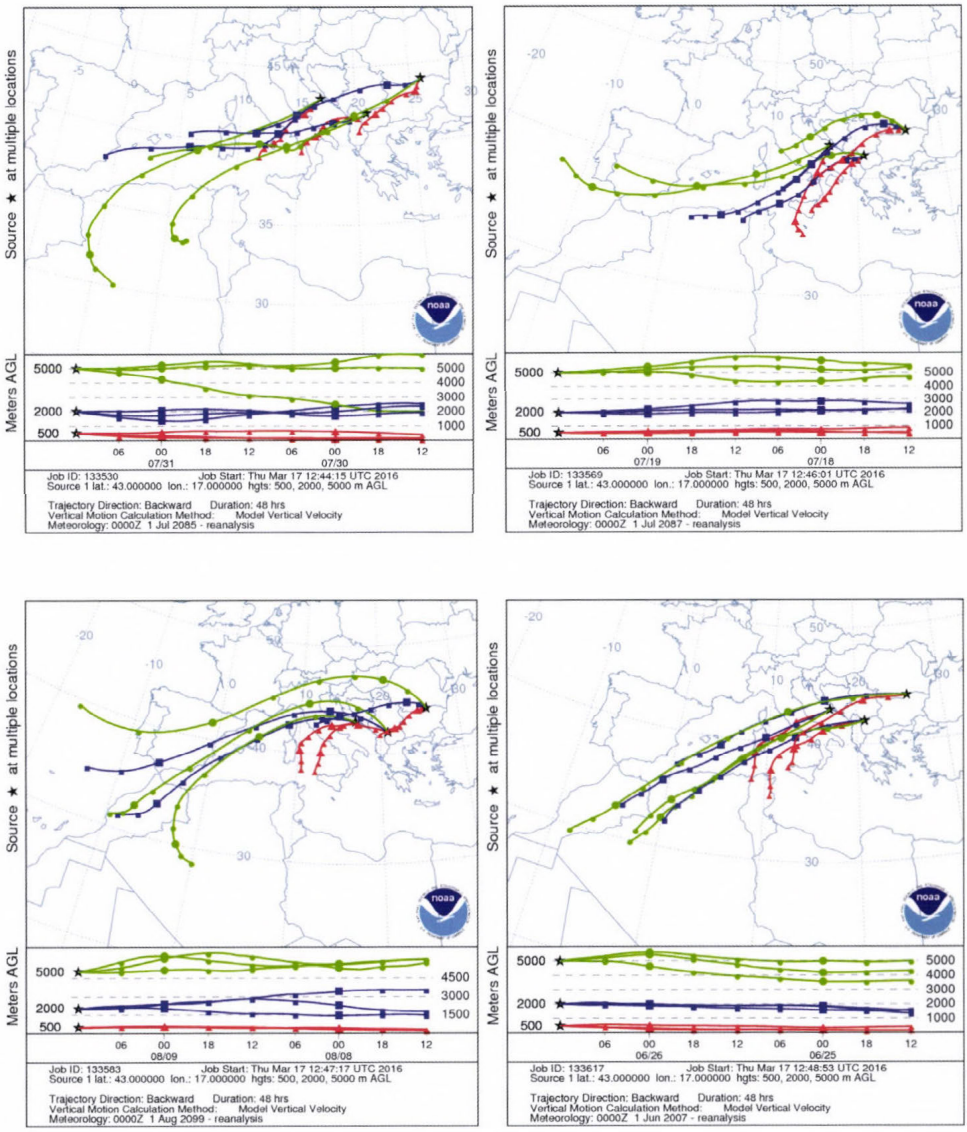

Fig. 9. 48-hour backward trajectories for the selected days in the synoptic type 2 causing HWs based on the reanalyses of the NOAA HYSPLIT model.

4. Discussion and summary

According to the research, in southeastern Europe between 1973 and 2010, there was an increase in Tmax in summer, which, averaged for the whole area, was 0.78 °C/10 years. A similar trend of changes in Tmax was also observed in central Europe (0.52 °C/10 years; *Tomczyk* and *Bednorz,* 2016) and northern Europe (0.38 °C/10 years; *Tomczyk et al.,* 2016). Within the analyzed area, similarly to other regions of Europe, the recorded increase was considerably influenced by changes in Tmax in the first decade of the 21st century, when Tmax generally exceeded the norm of the 1973–2010 multiannual period. The obtained results are consistent with previous research concerning air temperature changes in, among others, Greece (*Philandras et al.,* 2008; *Founda* and *Giannakopoulos,* 2009), Moldova (*Corobov et al.,* 2010), Romania (*Ionita et al.,* 2013), Serbia (*Bajat et al.,* 2015; *Unkašević and Tošić,* 2009), Slovenia (*de Luis et al.,* 2014; *Tošić et al.,* 2016), and the Mediterranean (*Efthymiadis et al.,* 2011).

The consequence of the increase in Tmax was an increasingly frequent occurrence of hot days and HWs. In the analyzed period, the rate of change in the number of hot days was 6.2 days/10 years. The observed changes are much more intensive than in central Europe (2.9 days/10 years; *Tomczyk* and *Bednorz,* 2016) and northern Europe (1.7 days/10 years; *Tomczyk et al.,* 2016). In the analyzed multiannual period, at most of the stations, both hot days and HWs were most numerous in the first decade of the 21st century. The obtained results are consistent with trends of changes found in Europe (*Gocheva et al.*, 2006; *Kyselý,* 2010; *Efthymiadis et al,* 2011; *Papanastasiou et al,* 2014; *Shevchenko et al.,* 2014; *Spinoni et al.,* 2015; *Unkašević* and *Tošić,* 2015; *Lakatos et al.,* 2016) and worldwide (*Batima et al.,* 2005; *Ding et al.,* 2010; *Pai et al.,* 2013; *Peterson et al.,* 2013; *Keggenhoff et al.,* 2015).

The occurrence of HWs in southeastern Europe was mostly connected with a well-developed ridge of high pressure settling over Europe, which caused an inflow of air masses from the northeast and east. Similar results were obtained by *Unkašević* and *Tošić* (2009) when they were analysing the occurrence of HWs in Serbia. The authors showed that HWs occurred most frequently during BM type according to the Grosswetterlagen (GWL) classification; therefore, with the presence of a ridge of high pressure over central Europe. Summer advection of continental air masses from the eastern sector also causes the occurrence of high temperatures and HWs in central Europe (*Wibig,* 2007; *Ustrnul et al.,* 2010; *Porębska* and *Zdunek,* 2013; *Tomczyk* and *Bednorz,* 2016).

The second circulation type conducive to the occurrence of HWs in southeastern Europe is connected with the occurrence of the Azores High over the continent and a low with its centre spreading from the North Sea to the Baltic Sea. Then, there was a weak pressure gradient recorded over the analyzed area. This situation was conducive to the advection of warm air masses from the

south and southwest. A similar circulation type was identified by *Unkašević* and *Tošić* (2011), who investigated the HW of 2007 in Serbia. During HWs, T850 positive anomalies were also observed, which were higher in type 2, and this confirms that advection of air masses from the southern sector is related to higher temperatures within the analyzed area than to advection from the northeast and east. The obtained results are consistent with previous research studies which have proven that the occurrence of extreme temperatures in southern Europe is caused by the inflow of air masses from over North Africa (*Domonkos et al.*, 2003; *Gocheva et al.*, 2006; *Unkašević* and *Tošić*, 2009).

Acknowledgements: This work was supported by the Polish National Science Centre under grant number: UMO-2014/15/N/ST10/00717.

References

Avotniece, Z., Rodinov, V., Lizuma, L., Briede, A., and *Kļaviņš, M.,* 2010: Trends in the frequency of extreme climate events in Latvia. *Baltica 23,* 135–148.

Bajat, B., Blagojević, D., Kilibarda, M., Luković J., and *Tošić I.,* 2015: Spatial analysis of the temperature trends in Serbia during the period 1961–2010. *Theor. Appl. Climatol. 121*, 289–301.

Barriopedro, D., Fischer, E.M., Luterbacher, J., Trigo, R.M., and *García-Herrera R.,* 2011: The hot summer of 2010: redrawing the temperature record map of Europe. *Science 332*, 220–224.

Batima, P., Natsagdorj, L., Gomboluudev, P., and *Erdenetsetseg B.,* 2005: Observed climate change in Mongolia. *AIACC Working Paper 13*, 4–25.

Bednorz, E., 2008: Synoptic conditions of snow occurrence in Budapest. *Meteorologische Zeit. 17,* 39–45.

Bednorz, E., 2011: Occurrence of winter air temperature extremes in Central Spitsbergen. *Theor. and Appl. Climatol. 106*, 547–556.

Bielec-Bąkowska, Z., 2014: Silne wyże nad Europą (1951-2010). *Wydawnictwo Uniwersytetu Śląskiego*, Katowice, 219. (in Polish)

Beniston, M., Stephenson, D.B., Christensen, O.B., Ferro, C.A.T., Frei, C., Goyette, S., Halsnaes, K., Holt, T., Jylha, K., Koffi, B., Palutikof, J., Scholl, R., Semmler, T., and *Woth, K.,* 2007: Future extreme events in European Climate: An exploration of regional climate model projections. *Climatic Change 81*, 81–95.

Bobvos, J., Fazekas, B., and *Páldy, A.,* 2015: Assessment of heat-related mortality in Budapest from 2000 to 2010 by different indicators. *Időjárás 119, 2*, 143–158.

Chromow, S.P., 1952: Meteorologia i klimatologia, Warszawa, *PWN*, 488. (in Polish)

Corobov, R., Sheridan, S., Overcenco, A., and *Terinte, N.,* 2010: Air temperature trends and extremes in Chisinau (Moldova) as evidence of climate change. *Climate Res. 42*, 247–256.

Ding, T., Qian, W.H., and *Yan Z.W.,* 2010: Changes of hot days and heat waves in China during 1961–2007. *Int. J. Climatol. 30*, 1452–1462.

de Luis, M., Čufar, K., Saz, M.A., Longares, L.A., Ceglar, A., and *Kajfež-Bogataj, L.,* 2014: Trends in seasonal precipitation and temperature in Slovenia during 1951–2007. *Regional Environmental Change 14*, 1801–1810.

Domonkos, P., Kyselý J., Piotrowicz, K., Petrovic, P., and *Likso, T.,* 2003: Variability of extreme temperature events in south-central Europe during the 20th century and its relationship with large-scale circulation. *Int. J. Climatol. 23*, 987–1010.

Efthymiadis, D., Goodess, C.M., and *Jones, P.D.,* 2011: Trends in Mediterranean gridded temperature extremes and large-scale circulation influences. *Nat. Haz. Earth Sys. Sci. 11*, 2199–2214.

Esteban, P., Jones, P.D., Martin-Vide, J., and *Mases, M.,* 2005: Atmospheric circulation patterns related to heavy snowfall days in Andorra, Pyrenees. *Int. J. Climatol. 25*, 319–329.

Frich, P., Alexander, L.V., Della-Marta, P., Gleason, B., Haylock, M., Klein Tank, A.M.G., and *Peterson T.,* 2002: Observed coherent changes in climatic extremes during 2nd half of the 20th century. *Climate Res. 19*, 193–212.

Founda, D., and *Giannakopoulos, C.,* 2009: The exceptionally hot summer of 2007 in Athens, Greece–a typical summer in the future climate? *Glob. Planet. Change 67,* 227–236.

Gocheva, A., Trifonova, L., Marinova, T. and *Bocheva, L.,* 2006: Extreme Hot Spells and Heat Waves on the Territory of Bulgaria. Paper presented in Water Observation and Information System for Decision Support, 23 - 26 May 2006, Ohrid, Republic of Macedonia.

Ionita, M., Rimbu, N., Chelcea, S., and *Patrut, S.,* 2013: Multidecadal variability of summer temperature over Romania and its relation with Atlantic Multidecadal Oscillation. *Theor. Appl. Climatol. 113,* 305–315.

IPCC (2007) Climate change: The physical science basis. Contribution of Working Group I to the Fourth Assessment Report of the Intergovernmental Panel in Climate Change. Cambridge University Press, Cambridge.

IPCC (2013), Climate change: The physical science basis. Contribution of Working Group I to the Fifth Assessment Report of the Intergovernmental Panel in Climate Change, Cambridge University Press, Cambridge.

Johnson, H., Kovats, R.S., McGregor, G., Stedman, J., Gibbs, M., and *Walton, H.,* 2005: The impact of the 2003 heat wave on daily mortality in England and Wales and the use of Rapid Weekly Mortality Estimates. *Eurosurveillance 10, 7-9*, 168–171.

Kalnay, E., Kanamistu, M., Kistler, R., Collins, W., Deaven, D., Gandin, L., Iredell, M., Saha, S., White, G., Woollen, J., Zhu, Y., Leetmaa, A., Reynolds, R., Chelliah, M., Ebisuzaki, W., Higgins, W., Janowiak, J., Mo, K.C., Ropelewski, C., Wang, J., Jenne, R. and *Joseph D.,* 1996: The NMC/NCAR 40–Year Reanalysis Project. *Bull. Amer. Met. Soc. 77*, 437–471.

Kažys, J., Stankūnavičius, G., Rimkus, E., Bukantis, A., and *Valiukas D.,* 2011: Long–range alternation of extreme high day and night temperatures in Lithuania. *Baltica 24, 2,* 71–82.

Keggenhoff, I., Elizbarashvili, M., and King, L., 2015: Heat Wave Events over Georgia since 1961: Climatology, Changes and Severity. *Climate 3,* 308–328.

Kejna, M., Araźny, A., Maszewski, R., Przybylak, R., Uscka-Kowalowska, J., and *Vizi, Z.,* 2009: Daily minimum and maximum air temperature in Poland in the years 1951–2005. *Bull. Geography – Physical Geography, Ser. 2/2009*, 35–56.

Koffi, B, and *Koffi, E.,* 2008: Heat waves across Europe by the end of the 21st century: multiregional climate simulations. *Climate Research 36*, 153–168.

Kossowska-Cezak, U., 2010: Fale upałów i okresy upalne - metody ich wyróżniania i wyniki zastosowania. *Prace Geograficzne 123*, 143–149. (in Polish)

Krzyżewska, A., 2010: Fale upałów jako zjawisko ograniczające turystykę w dużych miastach świata. *Krajobrazy rekreacyjne – kształtowanie, wykorzystanie, transformacja. Problemy Ekologii Krajobrazu XXVII,* 239–244. (in Polish)

Krzyżewska A., 2014: Warm and cold waves in South-Eastern (V) bioclimatic region in years 1981-2010. *Annales UMCS, Geographia, Geologia, Mineralogia et Petrographia 69, 2*, 143–154.

Kuchcik, M., and *Degórski, M.,* 2009: Heat– and cold–related mortality in the north–east of Poland as an example of the socio–economic effects of extreme hydrometeorological events in the Polish Lowland. *Geographia Polonica 82*, 1, 69–78.

Kürbis, K., Mudelsee, M., Tetzlaff, G., and *Brázdil R.,* 2009: Trends in extremes of temperature, dew point, and precipitation from long instrumental series from Central Europe. *Theor. Appl. Climatol. 98*, 187–195.

Kyselý, J., 2002: Temporal fluctuations in heat waves at Prague–Klementinum, the Czech Republic, from 1901–1997 and their relationships to atmospheric circulation. *Int. J. Climatol. 22*, 33–50.

Kyselý, J., 2010: Recent severe heat waves in central Europe: how to view them in a long–term prospect? *Int. J. Climatol. 30*, 89–109.

Lakatos, M., Bihari, Z., Szentimrey, T., Spinoni, J., Szalai, S., 2016: Analyses of temperature extremes in the Carpathian Region in the period 1961–2010. *Időjárás 120,* 41-51.

Meehl, G.A., and *Tebaldi C.,* 2004: More intense, more frequent, and longer lasting heat waves in the 21st century. *Science 305*, 994–997.

Migała, K., Urban, G., and *Tomczyński, K.,* 2016: Long-term air temperature variation in the Karkonosze mountains according to atmospheric circulation. *Theoretical and Applied Climatology125,* 337–351.

Mužíková, B., Vlček, V., and *Středa, T.,* 2011: Tendencies of climatic extremes occurrence in diff erent Moravian regions and landscape types. *ACTA Universitatis Agriculturae et Silviculturae Mendelianae Brunensis LIX, 5,* 169–178.

Niedźwiedź, T., 1981: Sytuacje synoptyczne i ich wpływ na zróżnicowanie przestrzenne wybranych elementów klimatu w dorzeczu górnej Wisły. *Rozprawy Habilitacyjne Uniwersytetu Jagiellońskiego* 58, Kraków. (in Polish)

Niedźwiedź, T., Łupikasza, E., and *Małarzewski, Ł.,* 2012 Wpływ cyrkulacji atmosfery na występowanie dni mroźnych w Hornsundzie (Spitsbergen). *Problemy Klimatologii Polarnej 22,* 17–26. (in Polish)

Pai D.S., Nair, S.A, and *Ramanathan, A.N.,* 2013: Long term climatology and trends of heat waves over India during the recent 50 years (1961–2010). *Mausam 64,* 4, 585–604.

Paldy, A. and *Bobvos, J.,* 2009: Impact of the Unusual Heatwave of 2007 on Mortality in Hungary. *Epidemiology 20, 6,* 126–127.

Papanastasious, D.K., Melas, D., and *Kambezidis, H.D.,* 2014: Heat waves characteristics and their relation to air quality in Athens. *Global Nest J. 16,* 919–928.

Peterson, T.C Heim, R.R., Hirsch, R., Kaiser, D.P., Brooks, H., Diffenbaugh, N.S., Dole, R.M., Giovannettone, J. P., Guirguis K.,. Karl, T.R., Katz, R.W., Kunkel, K., Lettenmaier, D., McCabe, G.J., Paciorek, C.J., Ryberg, K.R., Schubert, S., Silva, V.B.S., Stewart, B.C., Vecchia, A.V., Villarini, G., Vose, R.S., Walsh, J., Wehner, M., Wolock, D., Wolter, K., Woodhouse, C.A., and *Wuebbles, D.,* 2013: Monitoring and understanding changes in heat waves, cold waves, floods, and droughts in the United States: State of knowledge. *Bull. Amer. Met. Soc. 94,* 821–834.

Philandras, C., Nastos, P., and *Repapis, C.,* 2008: Air temperature variability and trends over Greece. *Global Nest J. 10,* 273–285.

Pongrácz, R., Bartholy, J., and *Bartha, E.B.,* 2013: Analysis of projected changes in the occurrence of heat waves in Hungary. *Adv. Geosci. 35,* 115–122.

Porębska, M., and *Zdune M.,* 2013: Analysis of extreme temperature events in Central Europe related to high pressure blocking situations in 2001–2011. *Met. Zeit. 22,* 533–540.

Poumadere, M., Mays, C., Le Mer, S., and *Blong, R.,* 2005: The 2003 Heat Waves in France: Dongerous Climate Change Here and Now. *Risk Analysis 25,* 1483–1494.

Revich, B.A., Shaposhnikov, D.A., Podol'naya, M.A., Khor'kova, T.L., and *Kvasha E.A.,* 2015: Heat Waves in Southern Cities of European Russia as a Risk Factor for Premature Mortality. *Studies on Russian Economic Development 26, 2,* 142–150.

Shaposhnikov, D., Revich, B., Bellander, T., Bedada, G.B., Bottai, M., Kharkova, T., and *et al.,* 2014: Mortality related to air pollution with the Moscow heat wave and wildfire of 2010. *Epidemiology 25,* 359–364.

Shevchenko, O., Lee, H., Snizhko, S., and *Mayer H.,* 2014: Long–term analysis of heat waves in Ukraine. *International J. Climatol. 34,* 1642–1650.

Spinoni, J., Lakatos, M., Szentimrey, T., Bihari, Z., Szalai, S., Vogt, J., and *Antofie T.,* 2015: Heat and cold waves trends in the Carpathian Region from 1961 to 2010. *Int. J. Climatol. 35,* 4197–4209.

Tomczyk, A.M., and *Bednorz, E.,* 2014: Heat and cold waves on the southern coast of the Baltic Sea. *Baltica 27,* 45–53.

Tomczyk, A.M., and *Bednorz, E.,* 2016: Heat waves in Central Europe and their circulation conditions. *Int. J. Climatol. 36,* 770–782.

Tomczyk, A.M., Piotrowski, P., and *Bednorz, E.,* 2016: Warm spells in Northern Europe in relation to atmospheric circulation. *Theor. Appl. Climatol.* DOI 10.1007/s00704-015-1727-0

Tošić, I., Zorn, M., Ortar, J., Unkašević, M., Gavrilov, M.B., and *Marković, S.B.,* 2016: Annual and seasonal variability of precipitation and temperatures in Slovenia from 1961 to 2011. *Atmos. Res. 168,* 220–233.

Unkašević, M., and *Tošić, I.,* 2009: An analysis of heat waves in Serbia, *Glob. Planetary Change 65,* 17–26.

Unkašević, M., and *Tošić, I.,* 2011: The maximum temperatures and heat waves in Serbia during the summer of 2007. *Climatic Change 108,* 207–223.

Unkašević, M., and *Tošić, I.*, 2015: Seasonal analysis of cold and heat waves in Serbia during the period 1949-2012. *Theor. Appl. Climatol. 120*, 29–40.

Ustrnul, Z., Czekierda, D., and *Wypych A.*, 2010: Extreme values of air temperature in Poland according to different atmospheric circulation classifications. *Physics Chemistry Earth 35*, 429–436.

Ward, J.H., 1963: Hierarchical grouping to optimize an objective function. *J. Amer. Statistical Assoc. 58*, 236–244.

Wibig, J., 2007: Fale ciepła i chłodu w środkowej Polsce na przykładzie Łodzi. *Acta Universitatis Lodziensis, Folia Geographica Physica 8*, 27–61. (in Polish)

Wilks, D.S., 1995: Statistical methods in the atmospheric sciences: an introduction. International geophysics series, vol. 59. Academic, New York, 464 pp.

Yarnal, B., 1993: Synoptic Climatology in Environmental Analysis. Belhaven Press, London.

Zacharias, S., Koppe, Ch., and *Mücke, H–G.*, 2015: Climate change effects on heat waves and future heat wave–associated IHD mortality in Germany. *Climate 3*, 100–117.

IDŐJÁRÁS

Quarterly Journal of the Hungarian Meteorological Service
Vol. 121, No. 1, January – March, 2017, pp. 415–430

Energy performance of the cooled amorphous silicon photovoltaic (PV) technology

Henrik Zsiborács[1*], Béla Pályi[1], Hegedűsné Nóra Baranyai[1], Mihály Veszelka[1], István Farkas[2], and Gábor Pintér[1]

[1] *University of Pannonia, Georgikon Faculty, Deák Ferenc Street 16, 8360 Keszthely, Hungary*

[2] *Szent Istvan University, Páter Károly Street 1, 2103 Gödöllő, Hungary*

**Corresponding author E-mail: ifj.zsiboracs.henrik@gmail.com*

(Manuscript received in final form February 1, 2016)

Abstract—In this paper, the effect of two types of water based cooling methods of amorphous silicon (a-Si) modules and a panel was studied in the summer period. One new (unused) and some 11-year-old a-Si modules and a panel with two different cooling techniques (sprinkling and flowing water cooling) were examined. Our reference for the evaluation was an unused a-Si module without any cooling. The results were analyzed from both statistical and technical aspects.

Key-words: solar energy, temperature dependence, water cooling, Z-test

1. Introduction

Renewable energies have an increasing role in the process of energy production (*Szabó et al.*, 2015, *Horváth et al.*, 2015). Besides numerous other benefits, energy production based on solar performances can significantly contribute to sustainable energy management. By a one-time investment in solar PV technology it is possible to produce CO_2-free, green energy for free without producing any waste for several decades (*Hosenuzzaman et al.*, 2015, *Aman et al.*, 2015).

The quantity of energy which can be produced by a solar PV module depends primarily on its type and composition and the joint effects of the

location and the current natural factors. Modules are tested and certified under laboratory conditions under which their nominal performances are established (STC-Standard Test Conditions, AM = 1.5 air pollution, 1000 W/m^2 solar radiation, and 25 °C module temperature). However, these conditions are not given during operation, so PV modules hardly ever produce their nominal performance (TÜV SÜD America Inc, 2015).

Due to their reliability, the market share of crystalline silicon PV modules is 85–90%, and their efficiency can reach 25.6% ± 0.5% in the case of monocrystalline modules and 20.8% ± 0.6% in the case of polycrystalline ones (*Green et al.*, 2015; IEA, 2014; *Cosme et al.*, 2015; Panasonic Corporation, 2014; *Verlinden et al.*, 2014).

The amorphous silicon solar module is a type of thin film PV solar module with an efficiency of up to 10.2% ± 0.3%. The market share of all thin film PV modules is 10–15%, but that of amorphous silicon solar modules within that is difficult to determine (*Green et al.*, 2015; IEA, 2014; *Matsui et al.*, 2013).

The temperature coefficient of thin film solar modules is better than that of crystalline ones. Thus, their use is favorable primarily in very hot, desert environments and in power stations (*Fábián,* 2015).

Several factors may influence the efficiency of the utilization of solar energy coming to the Earth. In the case of solar PV technologies, the fluctuation of module temperatures due to the change of air temperature and global radiation is one of the important factors (*Skoplaki* and *Palyvos,* 2009; *Hai Alami,* 2014). Under Hungarian climatic conditions, the temperature of solar PV modules can reach 60–70 °C on warm days, which results in a decrease of power generation in the module. For this problem, various cooling technologies may offer solutions.

According to *Bahaidarah et al.,* (2013), the performance of PV modules strongly depends on the actual module temperature. Generally it can be said that most of the incoming energy turns into thermal energy in the PV modules and is not utilized (*Chandrasekar et at.,* 2013). The arising quantity of heat gets lost, on the one hand, and causes additional losses in the short and long term, on the other hand, since the increase in the temperature of the modules reduces the efficiency of the system, and, thus, it reduces the quantity of electric energy produced, while, in the long run, they also accelerate the ageing of the PV modules (*Ndiaye et al.,* 2014; *Kahoul et al.*, 2014). The decrease in efficiency may vary depending on the type of the PV module. In the case of crystalline silicon PV modules, the efficiency characteristically decreases by 0.5%, while in the case of a-Si modules by 0.3% as a result of a 1 °C temperature rise (*Radziemska* and *Klugmann*, 2002).

Various active and passive cooling procedures are used in solar PV technology for controlling the operating temperatures of the modules (*Chandrasekar et al.*, 2015; *Elnozahy et al.*, 2015; *Du et al.,* 2012). Four groups

of the cooling techniques can be distinguished (*Chandrasekar et al.,* 2015; *Ji et al.*, 2008):

- air-based,
- water-based,
- refrigerant-based,
- heat pipe-based.

In the present study, the water-based (water spraying and water flow over the front) procedures are discussed. In the course of spraying with water, the temperature of cooled PV modules decreases significantly compared to modules without cooling (under identical circumstances) due to the phenomenon of evaporation (*Abdolzadeh* and *Ameri,* 2009).

2. Measurement site

In the present experiment, cooled and uncooled Kaneka amorphous silicon PV modules were examined under real meteorological circumstances. The measurements took place in the same location on 8 different days in August 2015 with 4 different settings:

- A: ground-mounted, unused PV module without cooling as control,
- B: ground-mounted, unused PV module with cooling (sprayed),
- C: ground-mounted, 11-year-old PV modules with cooling by flowing water over the module front,
- D: roof-mounted, 11-year-old PV panel (with 6 modules) with cooling by flowing water over the module front connected to the grid with an inverter (*Fig. 1*).

Long-term global radiation data were not available for our research. Thus, the economic data related to cooling the PV modules were calculated on the basis of the above-mentioned days.

The unused amorphous silicon PV modules were facing south with a tilt angle of 35°. For the measurements, two PicoLog data acquisition systems were used, one with 12 and one with 16 input channels. These instruments allowed second-based, continuous data recording by a personal computer. The advantage of the data acquisition devices used for this research is that several units can be connected to one computer and its software is flexible. Consequently, the incoming signs are simultaneously visible (*Zsiborács et al.*, 2015).

In the case of the control module – besides the voltage and the current –, the surface temperature was measured at one point (in the middle of the top third of the module).

Table 1. The parameters of the solar modules examined

Specifications	Amorphous silicon PVmodule (unused)	Amorphous silicon PVmodule (11-year-old)
Country of origin	Japan	Japan
Manufacturer/Distributor	Kaneka	Kaneka
Model	G-EA050	K54
Nominal output (Pm) (W)	50	54
Power output tolerance (%)	±10%	±10%
Maximum power voltage (Vmp) (V)	67	62
Maximum power current (Imp) (A)	0.75	0.87
Open circuit voltage (Voc) (V)	91.8	85
Short circuit current (Isc) (A)	1.19	1.14
Module dimensions (mm)	960×990×40	920×920×40

Fig. 1. The measurement site in Keszthely (*Zsiborács et al.*, 2015).

In the case of the sprayed amorphous PV module, the temperature was measured at two places. One sensor was placed in the middle of the top third of the a-Si module, and the other one was on the left side of the bottom third of the a-Si module. This article uses the data from the first sensor. The temperature of the sprayed water, the voltage, and the current were measured. The automation of the cooling system was controlled by a thermostat, which was connected to the surface of the middle of the top third of the PV module.

In order to save water, the spray heads sprinkled the unused amorphous silicon modules intermittently, using exactly the amount of water needed to replace the water evaporated (*Zsiborács et al.*, 2015). However, the location of the 11-year-old a-Si modules did not allow the application of the spraying method. That is why the technique of flowing water over the module front was used, creating a homogeneous water film.

The water got to the spray head through an ion-exchange resin water-softening appliance The water needed for the cooling of the a-Si modules was supplied by a domestic waterworks from a garden well with filtered groundwater (*Fig. 2*) (*Zsiborács et al.*, 2015).

Fig. 2. Schematic diagram of PV modules measuring point (*Zsiborács et al.*, 2015).

For measuring the temperatures, Pt 100 sensors were used with the help of the PicoLog devices (*Zsiborács et al.*, 2015). The calibration of the whole temperature measurement system was done using an LM 35 digital thermometer with a linear voltage change (+ 10.0 mV/°C, 0.1 V = 1 °C, 1 V = 100 °C) and an accuracy of ± 1/4 °C at room temperature and that of ± 3/4 °C between –55 and + 150 °C.

A Voltcraft VC607 professional multimeter, which was checked by an LT1021 device (10,000 V +–5 mV), was used for the calibration of the voltage and the current.

The humidity of the air was measured by a HYTE-ANA-1735 device. The global radiation was measured by a pyranometer (an Eppley Black and White Model 4–48, certified by the Hungarian Meteorological Service). The wind speed was measured by a JL-FS2, 4–20 mA, 3-spoon aluminium device. The electric signs from the measurements were transmitted to the PicoLog device (*Zsiborács et al.*, 2015). The pyranometer was placed next to the PV modules at a 35° angle (same as the PV modules). The air humidity and wind speed measurements took place at the side of the PV modules at a height of 80 cm (*Fig. 3*).

A True Maximum Point Seeking (TMPS) device, which maintained the maximum power point (MPP) was used for the measurements. The schematic diagram of the measurement point is shown in *Figs. 2, 3,* and *4*.

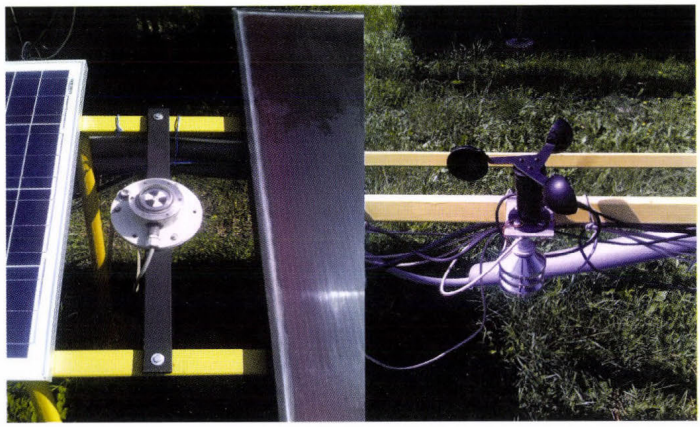

Fig. 3. The pyranometer, the wind speed sensor anemometer, and the humidity module.

Fig. 4. The unused amorphous silicon solar module measurement site in Keszthely.

A solar field consisting of 84 thin-film modules were used for the measurements of the 11-year-old a-Si modules, which had a nominal power of 4.5 kW. This system was set up at the same angle and location as the system above (*Fig. 5*). A Fronius Ig Tl inverter was used for the solar PV system.

Protection against TCO (transparent conductive oxide) corrosion, which can be caused by the chemical reaction of the water and the a-Si module if water gets under the glass, is important. If this problem is not prevented, the PV modules might go wrong in a couple of years (SMA Solar Technology AG, 2010). Grounding was impossible through the Tl inverter. However, the problem was solved by using a three-position switch. Silicone sealant was also applied to protect the PV modules between the glass and the frame.

The data from the 11-year-old modules were transmitted either to the PicoLog device or to the Fronius inverter. The control PV module was again an unused a-Si module.

The water needed for the PV module came from a domestic waterworks from a garden well with filtered underground water, after water softening.

For measuring the temperature of the 11-year-old amorphous silicon solar modules, a Lux Tools laser thermometer, which had been calibrated by a Pt100 sensor, was used. It was necessary to use the thermometer, since Pt100 sensors could not be used at the a-Si modules due to the limited number of channels of the measurement data collecting device.

The oscillation True Maximum Point Seeking device was suitable for receiving the data, because the voltage and current values were not far from each other. The a-Si modules examined are shown in *Fig. 5*, the first two columns on the left.

Fig. 5. The 11-year-old amorphous silicon solar panels

First the reaction of the six ground-mounted modules to cooling with flowing water over the module front was investigated one by one compared to that of the unused ones between 11.00 am – 12.15 pm on August 16, 2015. Each solar PV module examined was separated from the PV system and the parameters of the cooling were recorded one by one.

In the second phase the PV panel (with six a-Si modules) was studied (*Fig. 6*) in a way that only the panel was connected to the inverter. The other modules were disconnected at this time. That way the power surplus resulting from the cooling process could be measured. Here the TMPS solution, which was used in the first phase, could not be used. Thus, the data were supplied by the inverter.

Fig. 6. Amorphous silicon solar panel on the roof.

It is possible that the power changes in the control a-Si module due to natural effects during the period of the cooling process of the test modules. These changes have to be deducted from the power of the cooled amorphous silicon solar module.

The data were sampled hourly while spraying during sunny periods. The duration of cooling varied between 10 and 20 minutes depending on the measurement settings.

The surplus power was measured in the periods examined:

- before switching on spraying,
- at the end of the cooling period in a given hour.

Ten-minute cooling periods were sufficient for investigating the method of flowing water over the module.

The surplus power was measured in the periods examined:

- before switching on spraying,
- at the end of the cooling period in a given hour.

During the research, two-sample Z-tests were used to establish if there were any significant percentage differences in the performances of the cooled and the control PV modules.

3. Measured data and statistical analysis

In this chapter, the following issues are dealt with:

- regulation of the spraying water,
- the extra power produced by the unused and the 11-year-old amorphous silicon solar modules and panel,
- the actual daily energy production,
- hard water treatment.

3.1. The regulation of the spraying water at the unused a-Si module

The daily water consumption under operating conditions was examined on August 8, 2015.

In order to reduce water consumption, the spray heads were operated intermittently, thereby the system used minimal energy and only the amount of water necessary for evaporation. This way the efficiency of the spraying method could be determined for the amorphous silicon solar module.

By using the digital thermostat, a temperature regulating method that – depending on the temperature of the control module – can reduce the temperature of the surface of the cooled module by the average value of temperature reduction achievable in the given hour of the day was tested manually. Thus, the daily cooling period was maximally exploited.

In the case of the 50-W unused amorphous silicon solar module, 3 nozzles placed at a distance of 32 centimeters from each other were used. Depending on the weather, this system created a nearly homogenous sprayed surface (100 cm wide, 100 to 120 cm long) at 2 psi. From 9:00 am to 05:00 pm the water consumption was 4.2 l.

3.2. *Detecting extra performance produced by the sprayed unused amorphous silicon PV module*

The unused, test, and control PV modules were the same type and capacity according to the manufacturer's specifications. The relative changes in their performances were compared on August 7, 2015 (01:00 pm – 05:00 pm). The data were recorded every second. The two-sample Z-test established that the relative changes in the performances of the two unused modules were the same (P= 0.634).

Depending on the weather conditions (sunny weather), the measurements took place every hour between 09:00 am and 05:00 pm. This experiment involved 21 measurements. The average measurement data are shown in *Table 2*. By this test, the extra performance and temperature decrease of the PV module achievable by the sprinkling method were determined. It can be seen that the daily average extra performance increase of the unused amorphous silicon solar module was + 3.6% compared to the control a-Si module. Our tests support the results of *Skoplaki* and *Palyvos* of 2009, since in the case of the cooled a-Si module, an average performance increase of 0.3% for every 1-°C decrease in module temperature was observed.

Table 2. Data of the unused PV modules during spray cooling in August

Time (h)	**Average global radiation (W/m²)**	**Average wind speed (m/s)**	**Average air temperature (°C)**	**Average air humidity (%)**	**Sprayed a-Si module average temperatures decrease (°C)**	**Observed average extra power during spray cooling (%)**
9–10	455.45	0.2	28.0	38.0	7.3	2.6
10–11	679.3	0.2	27.2	37.0	12.7	4.0
11–12	771.5	0.1	30.5	37.0	13.5	3.4
12–13	904.8	0.3	29.0	37.0	14.4	4.1
13–14	925.7	0.4	32.9	35.8	17.4	4.8
14–15	928.5	0.2	32.6	36.4	15.1	3.3
15–16	816.3	0.0	29.4	37.8	15.1	3.6
16–17	641.8	0.5	28.3	37.5	12.4	3.0
Average						**3.6**
CV (%)						17.9

3.3. Detecting extra performance produced by the 11-year-old, ground-mounted a-Si modules cooled by water flow over the front

The testing of the 11-year-old a-Si modules took place on August 26, 2015 from 11:00 am to 12:15 pm.

In the first phase of the test, the relative change in the performance of the ground-mounted PV modules was examined over time without cooling compared to the unused module. Before the cooling experiment, all six a-Si modules were examined for 30 seconds each, one by one. The two-sample Z-test established that the relative change in the performance of the modules was the same (P= 0.759).

The cooling was done by water flow over the front. The averaged measurement data are shown in *Table 3*. In this test, the achievable extra performance and temperature decrease of the PV modules were determined. It can be seen that compared to the control a-Si module, the average performance increase of the 6 modules was 3.8% during the measurements. For the unused a-Si module this value was + 3.6%, meaning that the reaction to cooling was almost the same after 11 years of use.

Table 3. Data of the 11-year-old a-Si modules cooled by water flow over the front on August 26, 2015 (11:00-12:15)

Module	**Average global radiation (W/m^2)**	**Average wind speed (m/s)**	**Average air temperature (°C)**	**Average air humidity (%)**	**Sprayed a-Si module average temperatures decrease (°C)**	**Observed average extra power during cooling (%)**
1.	748.2	0.6	24.7	35.8	11.1	4.3
2.	767.7	0.5	25.5	36.0	14.1	3.4
3.	787.7	0.5	25.8	35.4	15.0	3.4
4.	816.3	0.3	26.6	35.0	12.5	4.0
5.	830.5	0.5	26.5	34.7	16.8	3.5
6.	844.1	0.5	26.2	35.5	14.3	4.3
Average						**3.8**
CV (%)						10.1

3.4. *Detecting extra performance produced by the 11-year-old a-Si panel connected to a grid-connected inverter*

The testing of the amorphous silicon panel took place on August 26, 2015 from 11:00 am to 2:00 pm. During the experiment only 6 a-Si modules were connected to the inverter. Thus, the extra power resulting from the water cooling effect could be detected more easily. During the experiment three tests were carried out, but the last measurement was not reliable due to changes in global radiation.

The Fronius inverter constantly checks the MPP and shows the changes in performance every 2 seconds. To establish the amount of extra performance during the first measurement, the average performance of the 1 minute before the start of cooling and the average performance in the last 1 minute of the cooling were used. The first test lasted for 8 minutes, during which the temperature of the a-Si module decreased by 18.3°C and the performance increased by 5.2% (*Table 4*).

During the second measurement, the average performance of the last 30 seconds before the start of cooling and the average performance in the last 1 minute of the testing process were used to establish the quantity of extra performance. The duration of the second measurement was 6 minutes, since the global radiation changed after that. During the test, the temperature of the amorphous silicon solar PV module decreased by 15.3 °C and the performance increased 3.8% (*Table 4*).

The grid-connected PV system tests showed that increases in power were detectable not only in PV modules but also in the inverter-connected 11-year-old amorphous silicon panel.

Table 4. Data of the 11-year-old a-Si panel cooled by water flow over the front on August 26, 2015 (13:00 – 14:00)

a-Si panel number of measurements	**Average global radiation (W/m^2)**	**Average wind speed (m/s)**	**Average air temperature (°C)**	**Average air humidity (%)**	**Sprayed a-Si module average temperatures decrease (°C)**	**Observed average extra power during cooling (%)**
1	887.5	0.2	27.5	36.3	18.3	5.2
2	880.4	0.2	26.9	36.9	15.3	3.8

3.5. The actually achievable daily energy production

The average extra performance data detected during the investigation of the unused a-Si module were projected onto an a-Si system (4.6 kW) located in Balatonudvari, since the measurement site in Keszthely undergoes two shady periods in the early morning and in the late afternoon, which could have distorted the results. On the two ideal summer days the examined PV system in Balatonudvari reached a peak performance of 3.4 kW and 3.3 kW between 1 pm. and 2 pm. That means that the actual performance was between 71.7% and 73.9% of the maximum performance theoretically achievable. Consequently, the inverter capacity was not completely utilized, which could provide an opportunity for increasing the performance by cooling (SZALONTAI Rendszerintegrátor Kft., 2015).

As seen above, the average performance increase of the unused cooled a-Si module was + 3.6% between 9 am and 5 pm. compared to the control amorphous silicon PV module, which means 3.6% more energy output during that period.

In the experiment, a domestic waterworks consuming 750 Wh energy (1800 l/hour, 30 l/min) was used. The pump did not have to operate all the time, since as a pressure tank, it also belonged to the system. For one a-Si module, 4.2 l of water and 1.75 Wh pump energy were used (from 9:00 am – 5:00 pm) during the cooling period.

For determining the daily energy actually produced the above-mentioned 4.6-kW a-Si PV system in Balatonudvari was used. The plant, situated at a distance of 44.6 km from Keszthely, is equipped with an online monitoring station with production data. In order to calculate the average daily production three ideal days were selected in August (August 01, 10, 28, 2015).

In *Table 5*, the energy production of the PV system determined for the given days on the basis of the available hourly actual energy production data series is shown. It was established that 6.5% of the average daily energy produced could not be used for cooling due to the characteristics of the cooling method, since no reaction to cooling was detectable before 09:00 am and after 05:00 pm. According to our measurements, a minimum global radiation of 450 W/m^2 at an air temperature of 20 °C and 390 W/m^2 at an air temperature of 30 °C is necessary to operate the cooling system. For this reason, the actual significance of water cooling for energy generation decreased from 3.6% to 3.4% on a daily basis. If the 1.75 Wh energy necessary for the pump is deducted from the energy produced daily, the actual energy gain decreases to 2.7%.

Table 5. Daily production data of the 4.6-kW PV field in Balatonudvari

Time (day)	Actual daily energy production (7-20) (kWh)	Energy produced during the cooling period (9-17) (kWh)	Released 3,6% extra energy during cooling period (9-17) (kWh)	Total energy production with cooling (kWh)	Actual extra energy during cooling period (kWh)	Daily amount of energy that cannot be used for cooling (%)	Actual daily extra energy (%)	Average daily extra energy (%)
Aug 1, 2015	25.0	23.3	24.2	25.9	0.8	7.3	3.4	
Aug 10, 2015	23.1	21.5	22.3	23.9	0.8	7.3	3.4	3.4
Aug 28, 2015	23.5	22.4	23.2	24.3	0.8	4.9	3.4	

3.6. Hard water treatment

The protection against limescale is necessary for the applied cooling method, since limescale is deposited on the glass surface of the PV modules. Ion-exchange polymers do not solve the problem completely. Therefore, it is advisable to apply a reverse osmosis water purifier.

4. Summary

Two different techniques (sprinkling and flowing water cooling) for cooling a-Si modules and a panel were examined in the summer period to establish their average extra performance increase thanks to the cooling process. The performance increase in the case of the cooled unused amorphous silicon solar module was +3.6% compared to the control a-Si module. Our experiments confirmed the results of *Skoplaki* and *Palyvos* of 2009, since in the case of the cooled a-Si module, an average performance increase of 0.3% for every 1-°C decrease in module temperature was observed.

It was found that compared to the control a-Si module, the average performance of the six cooled, 11-year-old, ground-mounted a-Si modules was 3.8% higher during the measurements. For the unused a-Si module this value was + 3.6%, meaning that the reaction to cooling was almost the same after 11 years of use.

The grid-connected PV system tests showed that increases in power were detectable not only in PV modules but also in the inverter-connected 11-year-old amorphous silicon panel.

Based on data from the PV system in Balatonudvari it was established, that 6.5% of the average daily energy produced could not be used for cooling due to the characteristics of the cooling method, since no reaction to cooling was detectable before 09:00 am and after 05:00 pm. According to our measurements, a minimum global radiation of 450 W/m^2 at an air temperature of 20 °C and 390 W/m^2 at an air temperature of 30 °C is necessary to operate the cooling system. For this reason, the actual significance of water cooling for energy generation decreased from 3.6% to 3.4% on a daily basis. If the 1.75 Wh energy necessary for the pump is deducted from the energy produced daily, the actual energy gain decreases to 2.7%.

References

Abdolzadeh, M. and *Ameri, M.,* 2009: Improving the effectiveness of a photovoltaic water pumping system by spraying water over the front of photovoltaic cells. *Renew. Energ. 34,* 91–96.

Aman, M.M., Solangi, K.H., Hossain, M.S., Badarudin, A., Jasmon G.B., and *Mokhlis H.,* 2015: A review of Safety. Health and Environmental (SHE) issues of solar energy system. *Renew. Sustain. Energy Rev. 41*, 1190–1204.

Bahaidarah, H., Subhan, A., Gandhidasan, P., and *Rehman S.,* 2013: Performance evaluation of a PV (photovoltaic) module by back surface water cooling for hot climatic conditions. *Energy 59*, 445–453.

Chandrasekar, M., Rajkumar, S., and *Valavan, D.,* 2015: A review on the thermal regulation techniques for non integrated flat PV modules mounted on building top. *Energy Buildings 86*, 692–7.

Chandrasekar, M., Suresh, S., Senthilkumar, T., Ganesh Karthikeyan, M., 2013: Passive cooling of standalone flat PV module with cotton wick structures. *Energ. Convers. Manage. 71*, 43–50.

Cosme, I., Cariou, R., Chen, W., Foldyna, M., Boukhicha, R., Cabarrocas, P.R.I., Lee, K.D., Trornpoukis, C., and *Depauw, V.,* 2015: Lifetime assessment in crystalline silicon: From nanopatterned wafer to ultra-thin crystalline films for solar cells. *Solar Energ. Materials Solar Cells 135*, 93–98.

Du, B., Hu, E., and *Kolhe, M.,* 2012: Performance analysis of water cooled concentrated photovoltaic (Cphotovoltaic) system. *Renew. Sustain. Energy Rev. 16*, 6732–6736.

Elnozahy, A., Rahman, A.K.A., Ali, A.H.H., Abdel-Salam, M., and *Ookawara, S.,* 2015: Performance of a PV module integrated with standalone building in hot arid areas as enhanced by surface cooling and cleaning. *Energy Buildings 88*, 100–109.

Fábián, T., 2015: A Rádiótechnika Évkönyve 2015. *Rádióvilág Kft.* HU-ISSN 0557-6229, 101–107.

Green, M.A., Emery, K., Hishikawa, Y, Warta, W., and *Dunlop, E.D.,* 2015: Solar cell efficiency Tables (Version 45). *Progr. Photovoltaics Res Appl. 23*, 1–9.

Hai Alami, A., 2014: Effects of evaporative cooling on efficiency of photovoltaic modules. *Energy Conv. Manage. 77*, 668–679.

Horváth, M., Kassai-Szoó, D., and *Csoknyai, T.,* 2016: Solar energy potential of roofs on urban level based on building typology. *Energy Buildings 111,* 278–289.

Hosenuzzaman, M., Rahim, N.A., Selvaraj, J., Hasanuzzaman, M., Malek, A.B.M.A., and *Nahar, A.,* 2015: Global prospects. progress policies and environmental impact of solar photovoltaic power generation. . *Renew. Sustain. Energy Rev. 41*, 284–97

Ji, J., Pei, G., Chow, T.T., Liu, K., He, H., Lu, J., and *Han, C.,* 2008: Experimental study of photovoltaic solar assisted heat pump system. *Solar Energy 82*, 43–52.

Kahoul, N., Houabes, M., and *Sadok, M.,* 2014: Assessing the early degradation of photovoltaic modules performance in the Saharan region. *Energy Conv. Manage. 82*, 320–326.

Matsui, T., Sai, H., Suezaki, T., Matsumoto, M., Saito, K., Yoshida, I., and *Kondo M.,* 2013: Development of highly Stable and efficient amorphous silicon based solar cells. Proc. 28th European Photovoltaic Solar Energy Conference. 2213–2217.

Ndiaye, A., Kebe, C.M.F., Charki, A., Ndiaye, P.A., Sambou, V., and *Kobi A.,* 2014: Degradation evaluation of crystalline-silicon photovoltaic modules after a few operation years in a tropical environment. *Solar Energy 103,* 70–77.

Panasonic Corporation, 2014: Panasonic HIT® Solar Cell Achieves World's Highest Energy Conversion Efficiency of 25.6% at Research Level Available at: news.panasonic.com/press/news/official.,data/data.dir/2014/04/en140410-4/en140410-4.html.Downloaded: 21.11.2015

Radziemska, E. and *Klugmann, E.,* 2002: Thermally affected parameters of the current–voltage characteristics of silicon photocell. *Energy Conv. Manage. 43,* 1889–1900.

Skoplaki, E. and *Palyvos, J.A.,* 2009: On the temperature dependence of photovoltaic module electrical performance: A review of efficiency/power correlations. *Solar Energy 83,* 614–624.

Skoplaki, E. and *Palyvos, J.A.,* 2009: Operating temperature of photovoltaic modules: A survey of pertinent correlations. *Renew Energy 34,* 23–29.

SMA Solar Technology AG., 2010. Module Technology - SMA inverters provide the optimum solution for every module. Duennschicht-TI-UEN114630|Version 3.0. 1–7. Available at: files.sma.de/dl/7418/Duennschicht-TI-UEN114630.pdf. Downloaded: 21.11.2015

Szabó, Sz., Enyedi, P., Horváth, M., Kovács, Z., Burai, P., Csoknyai, T., and *Szabó, G.,* 2015: Automated registration of potential locations for solar energy production with Light Detection And Ranging (LiDAR) and small format photogrammetry. *J. Cleaner Product 112,* 3820–3829.

SZALONTAI Rendszerintegrátor Kft. Balatonudvari PV system. 2015: Available at: www.sunnyportal.,com/Templates/PublicPageOverview.aspx?page=294cb041-aece-4668-93e3-fa9a4c89fbcc&plant=152c508b-dca1-48b7-9258-3f32e8574bfa&splang=en-US.Downloaded: 21.11.2015

TÜV SÜD America Inc., 2015. Basic Understanding of IEC Standard Testing For Photovoltaic Panels. Regan Arndt and Dr. Ing Robert Puto TÜV SÜD Product Service. 1–15. Available at: www.tuvamerica.com/services/photovoltaics/articlebasicunderstandingphotovoltaic.pdf. Downloaded: 21.11.2015

Verlinden, P., Deng, W., Zhang, X., Yang, Y., Xu, J., Shu, Y., Quan, P., Sheng, J., Zhang, S., and *Bao, J.,* 2014: Strategy, development and mass production of high-efficiency crystalline Si PV modules, in: 6th World Conference on Photovoltaic Energy Conversion, Kioto, Japan, 2014.

Zsiborács, H., Pályi, B., and *Pintér, G.,* 2015: Permetezett monokristályos napelemek vizsgálata. LVII. Georgikon Napok. 505–514.

IDŐJÁRÁS

VOLUME 120 * 2016

EDITORIAL BOARD

ANTAL, E. (Budapest, Hungary)
BARTHOLY, J. (Budapest, Hungary)
BATCHVAROVA, E. (Sofia, Bulgaria)
BRIMBLECOMBE, P. (Norwich, U.K.)
CZELNAI, R. (Dörgicse, Hungary)
DUNKEL, Z. (Budapest, Hungary)
FISHER, B. (Reading, U.K.)
GERESDI, I. (Pécs, Hungary)
HASZPRA, L. (Budapest, Hungary)
HORVÁTH, Á. (Siófok, Hungary)
HORVÁTH, L. (Budapest, Hungary)
HUNKÁR, M. (Keszthely, Hungary)
LASZLO, I. (Camp Springs, MD, U.S.A.)
MAJOR, G. (Budapest, Hungary)
MÉSZÁROS, E. (Veszprém, Hungary)
MÉSZÁROS, R. (Budapest, Hungary)
MIKA, J. (Budapest, Hungary)
MERSICH, I. (Budapest, Hungary)
MÖLLER, D. (Berlin, Germany)
PINTO, J. (Res. Triangle Park, NC, U.S.A.)
PRÁGER, T. (Budapest, Hungary)
PROBÁLD, F. (Budapest, Hungary)
RADNÓTI, G. (Budapest, Hungary)
S. BURÁNSZKI, M. (Budapest, Hungary)
SZALAI, S. (Budapest, Hungary)
SZEIDL, L. (Budapest, Hungary)
SZUNYOGH, I. (College Station, TX, U.S.A.)
TAR, K. (Debrecen, Hungary)
TÄNCZER, T. (Budapest, Hungary)
TOTH, Z. (Camp Springs, MD, U.S.A.)
VALI, G. (Laramie, WY, U.S.A.)
WEIDINGER, T. (Budapest, Hungary)

Editor-in-Chief
LÁSZLÓ BOZÓ

Executive Editor
MÁRTA T. PUSKÁS

BUDAPEST, HUNGARY

AUTHOR INDEX

TABLE OF CONTENTS

I. Papers

II. News

A

B

C

D

E

F

G

H

I

L

M

N

O

P

R

S

T

U

V

W

Z

INSTRUCTIONS TO AUTHORS OF *IDŐJÁRÁS*

The purpose of the journal is to publish papers in any field of meteorology and atmosphere related scientific areas. These may be

- research papers on new results of scientific investigations,
- critical review articles summarizing the current state of art of a certain topic,
- short contributions dealing with a particular question.

Some issues contain "News" and "Book review", therefore, such contributions are also welcome. The papers must be in American English and should be checked by a native speaker if necessary.

Authors are requested to send their manuscripts to

Editor-in Chief of IDŐJÁRÁS
P.O. Box 38, H-1525 Budapest, Hungary
E-mail: journal.idojaras@met.hu

including all illustrations. MS Word format is preferred in electronic submission. Papers will then be reviewed normally by two independent referees, who remain unidentified for the author(s). The Editor-in-Chief will inform the author(s) whether or not the paper is acceptable for publication, and what modifications, if any, are necessary.

Please, follow the order given below when typing manuscripts.

Title page: should consist of the title, the name(s) of the author(s), their affiliation(s) including full postal and e-mail address(es). In case of more than one author, the corresponding author must be identified.

Abstract: should contain the purpose, the applied data and methods as well as the basic conclusion(s) of the paper.

Key-words: must be included (from 5 to 10) to help to classify the topic.

Text: has to be typed in single spacing on an A4 size paper using 14 pt Times New Roman font if possible. Use of S.I. units are expected, and the use of negative exponent is preferred to fractional sign. Mathematical formulae are expected to be as simple as possible and numbered in parentheses at the right margin.

All publications cited in the text should be presented in the *list of references*, arranged in alphabetical order. For an article: name(s) of author(s) in Italics, year, title of article, name of journal, volume, number (the latter two in Italics) and pages. E.g., *Nathan, K.K.,* 1986: A note on the relationship between photosynthetically active radiation and cloud amount. *Időjárás 90,* 10-13. For a book: name(s) of author(s), year, title of the book (all in Italics except the year), publisher and place of publication. E.g., *Junge, C.E.,* 1963: *Air Chemistry and Radioactivity.* Academic Press, New York and London. Reference in the text should contain the name(s) of the author(s) in Italics and year of publication. E.g., in the case of one author: *Miller* (1989); in the case of two authors: *Gamov* and *Cleveland* (1973); and if there are more than two authors: *Smith et al.* (1990). If the name of the author cannot be fitted into the text: *(Miller,* 1989); etc. When referring papers published in the same year by the same author, letters a, b, c, etc. should follow the year of publication.

Tables should be marked by Arabic numbers and printed in separate sheets with their numbers and legends given below them. Avoid too lengthy or complicated tables, or tables duplicating results given in other form in the manuscript (e.g., graphs).

Figures should also be marked with Arabic numbers and printed in black and white or color (under special arrangement) in separate sheets with their numbers and captions given below them. JPG, TIF, GIF, BMP or PNG formats should be used for electronic artwork submission.

More information for authors is available: journal.idojaras@met.hu

Published by the Hungarian Meteorological Service

Budapest, Hungary

INDEX 26 361

HU ISSN 0324-6329